frontiers in Earth Science

ORIGINAL RESEARCH
published: 02 March 2022
doi: 10.3389/feart.2022.816922

Vertical Slip Rates of Normal Faults Constrained by Both Fault Walls: A Case Study of the Hetao Fault System in Northern China

Dongsheng Xu[1], Zhongtai He[1,2,3,4], Baoqi Ma[1], Jianyu Long[5], Hao Zhang[6] and Kuan Liang[1]*

[1]National Institute of Natural Hazards, Ministry of Emergency Management of China, Beijing, China, [2]Key Laboratory of Earthquake Dynamics of Hebei Province, Institute of Disaster Prevention, Langfang, China, [3]Key Laboratory of Crustal Dynamics, China Earthquake Administration, Beijing, China, [4]Southern Yunan Observatory for Cross-Block Dynamic Process, Yuxi, China, [5]Earthquake Administration of Sichuan Province, Chengdu, China, [6]Earthquake Administration of Jiangsu Province, Nanjing, China

The slip rate is a fundamental kinematic parameter of active faults. Traditional methods using fault scarps or trenches may produce inaccurate estimates of a fault's vertical slip rate. A normal fault's vertical slip rate requires constraints from the hanging wall and footwall. Here, the vertical slip rate at each measuring point along the fault was calculated by the joint constraints of terraces in the footwall and boreholes in the hanging wall. Nine measuring points were selected along the Sertengshan piedmont fault. The vertical slip rates of this fault since 65 and 12 ka were 0.74–1.81 and 0.86–2.28 mm/a, respectively. Four measuring points were selected along the Wulashan piedmont fault. The vertical slip rates of this fault since 60 and 12 ka were 2.14–3.11 and 1.84–2.91 mm/a, respectively. Seven measuring points were selected along the Daqingshan piedmont fault; the vertical slip rates were 2.5–3.88 and 1.78–2.83 mm/a since 58 and 11 ka, respectively. Analysis of the slip rates, the elapsed time since the last palaeoearthquake and the mean recurrence interval of palaeoearthquakes on each fault segment on the northern margin of the Hetao Basin suggests that the Langshankou and Hongqicun segments of the Sertengshan piedmont fault are at higher risk of earthquakes than the other segments. Among the fault segments of the Wulashan piedmont fault, the Baotou segment is at the highest seismic risk. The seismic risk of the Tuyouxi segment of the Daqingshan piedmont fault should not be ignored, and the Tuzuoxi, Bikeqi and Hohhot segments have high seismic risk. Based on the findings and a dynamic model of the formation and evolution of the Ordos block, it is concluded that the depositional centre of the Hetao Basin has tended to migrate from west to east. The vertical force generated by deep material movement is the dominant factor leading to a greater vertical slip rate in the eastern portion of the northern margin of the Hetao Basin. The modern stress field in the Hetao Basin results in an increase in the vertical slip rate of active faults from west to east along the northern margin of the basin.

Keywords: vertical slip rate, geological borehole, fault displacement, Hetao basin, marker strata, terrace

OPEN ACCESS

Edited by:
Wenjun Zheng,
Sun Yat-sen University, China

Reviewed by:
Haiyun Bi,
China Earthquake Administration, China
Yanxiu Shao,
Tianjin University, China

****Correspondence:***
Zhongtai He
hezhongtai@126.com

Specialty section:
This article was submitted to Structural Geology and Tectonics, a section of the journal Frontiers in Earth Science

Received: *17 November 2021*
Accepted: *14 February 2022*
Published: *02 March 2022*

Citation:
Xu D, He Z, Ma B, Long J, Zhang H and Liang K (2022) Vertical Slip Rates of Normal Faults Constrained by Both Fault Walls: A Case Study of the Hetao Fault System in Northern China. Front. Earth Sci. 10:816922. doi: 10.3389/feart.2022.816922

1 INTRODUCTION

The slip rate is a very important kinematic parameter of active faults and an important index for evaluating the seismic risk of faults. It refers to the velocity of fault dislocation over a certain period of time and represents the long-term and average activity level of the fault (Zhang et al., 2013; Zhang et al., 2017). It can be used to quantitatively compare the relative activity of different fault zones or the same fault zone in different periods and is also a very important parameter for seismic risk evaluation. Accurately obtaining the fault displacement amplitude is difficult, and accurately determining the rate of normal fault vertical slip requires constraints from the footwall and the hanging wall. However, because the strata of the hanging wall are buried underground by sedimentary cover when normal faults form, only the characteristics of the footwall strata exposed by surface faulting can be observed in the field, and it is difficult to find direct indicators of fault displacement. When calculating the slip rate, people usually consider only footwall strata and ignore the information of hanging wall strata buried underground, which leads to underestimating the slip rate of the fault and reducing the expected seismic risk of the fault.

Taking the fault system on the northern margin of the Hetao Basin, China, as an example, the vertical slip rate of the normal fault is constrained by terraces in the footwall of the fault and boreholes in the hanging wall of the fault. Located between the Yinshan fault block and Ordos block (Deng et al., 1999; Feng et al., 2015), the Hetao Basin is an important part of the peripheral Ordos fault basin belt and seismic belt. The northern margin fault system consists of the Sertengshan piedmont fault, Wulashan piedmont fault and Daqingshan piedmont fault from west to east and has controlled the formation and development of the Hetao Basin. The Hetao Basin experienced earthquakes with magnitudes of M7.5–M8 in 849 AD and M8 in 7 BC (He et al., 2018). In the 20th century, the Bikeqi earthquake in 1929 (M6.0), the Wuyuan earthquake in 1934 (M6.75), the Lingeer earthquake in 1976 (M6.3), the Bayinmuren earthquake in 1976 (M6.2), the Wuyuan earthquake in 1979 (M6.0) and the Baotou earthquake in 1996 (M6.0) (**Figure 1**) successively occurred in the fault zone; some small earthquakes of magnitude 4–5 have also occurred. Such earthquakes are distributed in the fault zone and are obviously controlled by major active faults at the boundary (Chen, 2002).

Since the 1990s, studies have investigated the vertical slip rate of the fault system on the northern margin of the Hetao Basin. The vertical slip rate of the Sertengshan piedmont fault has been 0.88–3.6 mm/a since the late Pleistocene and 0.19–2.2 mm/a during the Holocene (Institute of Crustal and Dynamics and China Earthquake Administration, 1995; Yang et al., 2002); the uplift rate of the Wulashan piedmont fault has been 0.5–2.0 mm/a since the late Pleistocene and 0.4–1.0 mm/a during the Holocene (Ma et al., 1998); and the vertical slip rate of the Daqingshan piedmont fault has been 2.61–4.49 mm/a since the late Pleistocene and 0.37–1.72 mm/a during the Holocene (Wu et al., 1996). In these previous studies, the fault slip rate was calculated considering only the footwall uplift height, that is, the footwall uplift rate, rather than the complete vertical slip rate of the fault. This approach leads to an underestimation of fault activity and earthquake risk.

In this paper, based on chronological data from marker strata, accurate vertical slip rates are calculated. The kinematic parameters of the faults in the late Quaternary were quantitatively studied by using boreholes in the hanging wall and terraces in the footwall, and the activity characteristics of the fault system in the late Quaternary and the seismic risk in the future were analysed and summarized.

2 REGIONAL SEISMIC TECTONIC SETTING

The Ordos block is located on the northeastern Tibetan Plateau. Due to the continuous influence of the uplift of the Tibetan Plateau and the subduction of multiple plates in the east, faults with different faulting intensities developed in different periods of the Cenozoic and formed a series of graben basins (Deng et al., 1999). The Hetao Basin between the northern margin of the Ordos block and the Yinshan (**Figure 1**) developed in the Oligocene mainly under the action of the maximum principal compressive stress field oriented in the ENE direction and has accumulated sediments since the early Neogene (Research Group of Active Fault System around Ordos Massif, 1988). Geomorphologically, the striking features of the Hetao fault zone are normal fault tectonic landforms: fault-formed terraces, fault scarps, river terraces, etc. (Wang and He, 2020). From west to east, the fault systems on the northern margin of the Hetao fault zone are the Sertengshan piedmont fault, the Wulashan piedmont fault and the Daqingshan piedmont fault. The Sertengshan piedmont fault extends from Langshan Pass in the west, extends nearly east–west to Wubulangkou, then turns to 120° and continues to the southeast until disappearing to the east of Wulanhudong, with a total length of approximately 150 km. The fault can be divided into four segments from west to east: the Langshankou segment (East Wugai-Dahoudian), the Hongqicun segment (Dahoudian-Wubulangkou) with an E-W trend, the Kuluebulong segment (Wubulangkou-Wayaotan) with a NW trend, and the Dashetai segment (Wulyaotan-Tailiang) (Long et al., 2017). The Wulashan piedmont fault starts at Wulateqianqi in the west and ends in northern Kundulun District in Baotou city in the east. The overall trend is nearly east–west, and the total length is approximately 110 km. It can be divided into three segments from west to east: the eastern segment of Wulateqianqi (Wulateqianqi-Gongmiaozi), the Gongmiaozi segment (Gongmiaozi-Heshunzhuang) and the eastern segment of Baotou (Heshunzhuang-Baotou) (Ma et al., 1998; Institute of Crustal and Dynamics and China Earthquake Administration, 2013). The Daqingshan piedmont fault extends from Zhaojunfen on the south bank of the Yellow River in Baotou in the west to the Kuisu area east of Hohhot in the east, with a total length of approximately 200 km. It has a general trend of ENE and a dip to the south with an angle of 45°–75° (He, 2006; Liu, 2012). It is a very important active fault in the Hetao fault zone. It can be divided into five segments from west to east: the Baotou segment (Yellow River-Xuehaigou), the Tuyouxi segment (Xuehaigou-Tuyouqi),

the Tuzuoxi segment (Tuyouqi-Tuzuoqi), the Bikeqi segment (Tuzuoqi-Wusutu) and the Hohhot segment (Wusutu-Kuisu) (Wu et al., 1996; He et al., 2007) (**Figure 1**). In this paper, nine measuring points along the Sertengshan piedmont fault, four along the Wulashan piedmont fault, and seven along the Daqingshan piedmont fault were selected to calculate the vertical slip rates of three active faults on the northern margin of the Hetao Basin since the late Pleistocene and Holocene.

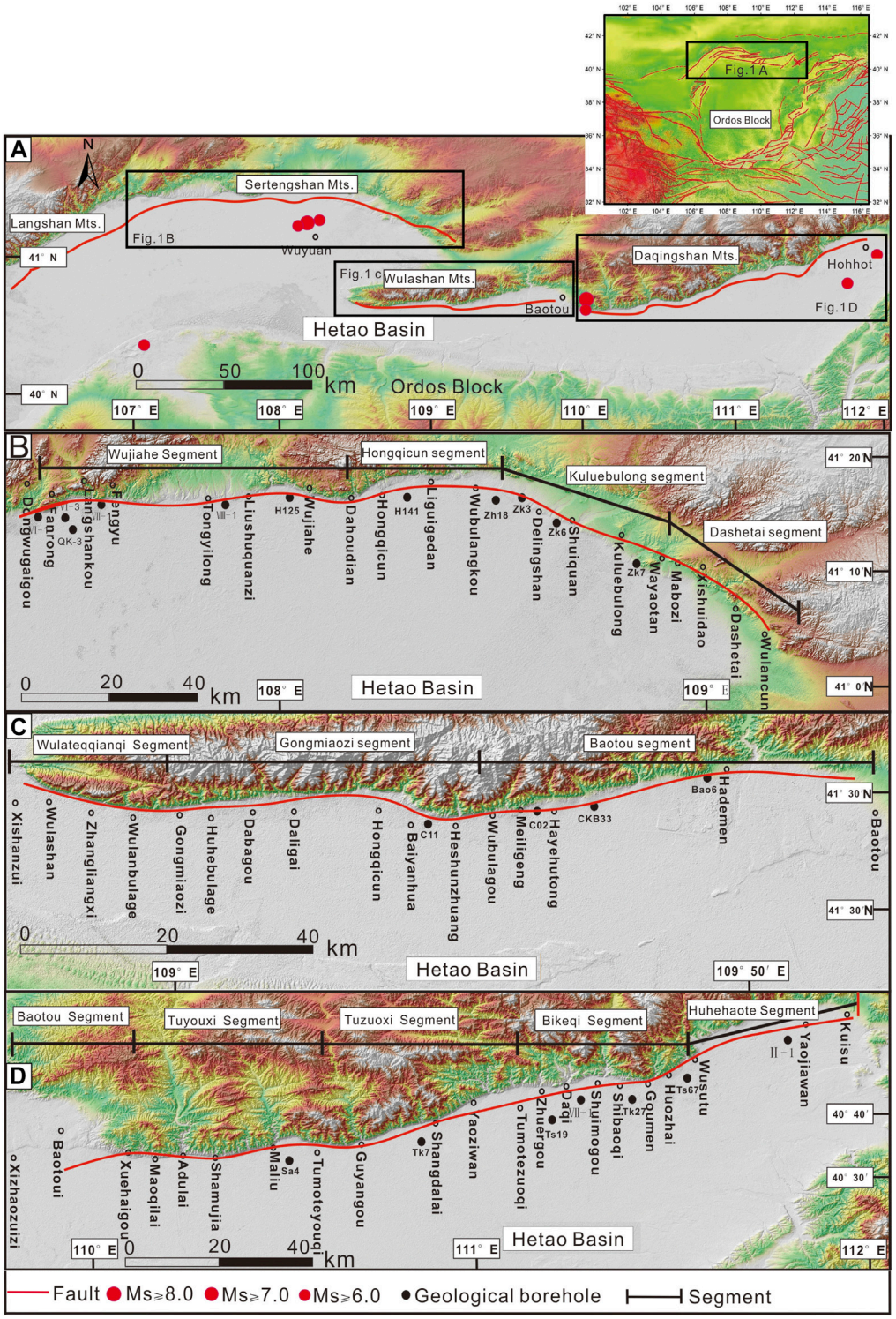

FIGURE 1 | Regional geological structure map: **(A)** Locations of the three faults; **(B)** Distribution of the Sertengshan piedmont fault; **(C)** Distribution of the Wulashan piedmont fault; **(D)** Distribution of the Daqingshan piedmont fault.

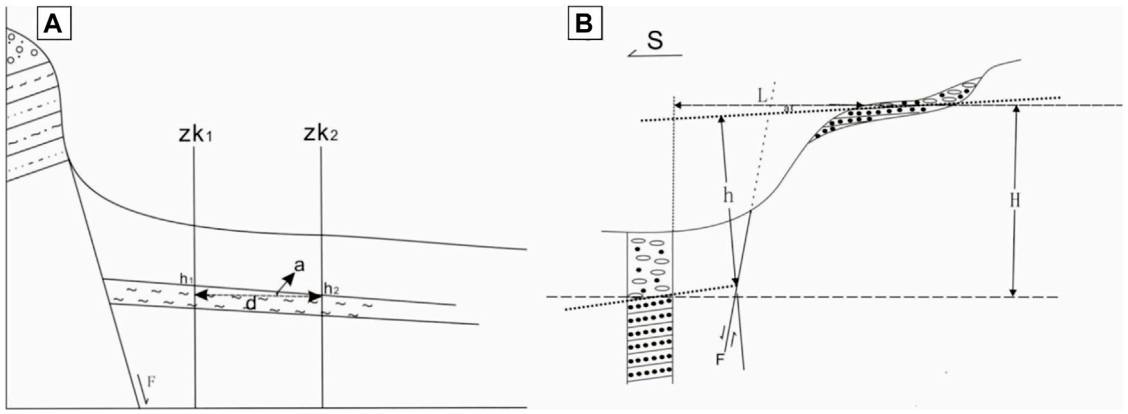

FIGURE 2 | (A) Calculation and calibration of vertical displacement amplitude (modified from Wu et al., 1996); **(B)** Calculation diagram of dip angle α of a marker strata.

3 METHODS

3.1 Vertical Displacement Calculation Method

The vertical displacement of a normal fault must be determined by comparing the same strata on both walls of the fault. The footwall terrace on the Hetao fault system has well-preserved stratigraphic outcrops, but the same strata in the hanging wall have been dissected and buried tens of metres below the surface. Therefore, only the stratigraphic sequence revealed by the borehole in the hanging wall of the fault can be compared to obtain more accurate fault displacement estimates. For the correlation between terrace strata and borehole strata, marker strata should be chosen first. The marker strata should meet the following conditions: (1) special lithology and special sedimentary tectonic strata or special interlayer interfaces; (2) no or very few similar layers or interfaces appear in the longitudinal direction; (3) the strata or interfaces are distributed stably in the lateral direction with little change in lithology or thickness; and (4) obvious features that are easy to identify. In addition to the correlation of marker strata, the ages of strata should be combined so that the activity rate can be calculated more accurately (Wu et al., 1996).

The vertical displacement obtained from the elevation difference of a marker strata is accurate only when the marker strata is horizontal. However, according to the field observations, all strata in this area have certain inclination angles, so it was necessary to calibrate the displacement obtained, as shown in **Figure 2A**. The real displacement can be calculated as follows: $h = (H - L \tan \alpha) \cos \alpha$, where L is the distance between the borehole and the terrace and α is the dip angle of the marker strata at the fault. H and L can be measured according to the elevation and distance of the borehole and the terrace, while a is measured according to the maker strata in the adjacent borehole near the fault.

However, according to the formula $h = (H - L \tan a) \cos \alpha$, L has little effect, while α has a great effect on the correction of the vertical displacement. The α referred to by Wu et al. (1996) is obtained from the field estimation of the dip angle of the marker strata in the terrace profile, which is quite different from the dip angle of the borehole lacustrine strata in the basin. In this paper, the ratio of the elevation difference between the borehole maker strata (m) and the spacing between boreholes (d) in the basin is adopted to calculate the dip angle of the maker strata, namely, $\alpha = \arctan(m/d)$, as shown in **Figure 2B**.

Additionally, h1-h2 = m

$\tan \alpha = m/d$

$a = \arctan(m/d)$

3.2 Real-Time Kinematic Field Terrace Survey

With the development of measurement technology, GPS RTK technology has gradually been applied to surveying and mapping in various industries (Wang et al., 2011). A Trimble R10 global navigation satellite system (GNSS) was used in this work. The system is a multichannel, multiband GNSS that integrates receivers, antennas and digital transmission stations. The horizontal accuracy of the instrument can reach ±10 mm + 1 ppm, and the vertical accuracy can reach ±20 mm + 1 ppm under the RTK measurement mode. The initialization time is generally less than 10 s, and the initialization reliability is greater than 99.9%. Based on a large number of field explorations, field investigations and comprehensive remote sensing interpretations, to accurately determine the relative height of the terrace, the distribution of the terrace and the height of the steep ridge on the footwall of the fault on the northern margin of the Hetao Basin were systematically measured, and a large-scale topographic map was produced in this study.

3.3 Drilling and Terrace Chronological Methods

To obtain a complete stratigraphic age profile since the late Pleistocene on the hanging wall of the fault, drilling was

performed within 3 km of the fault, and the cores were described and sampled. The type of drilling rig used in this drilling was an XY-300, and the depth of a single hole was generally less than 100 m. During drilling, the holes were required to cross the fault, and the elevation of the top of the holes was recorded. After the core was removed, the bottom of each section of the core was marked with labels to indicate the depth and lithologic characteristics drilled thus far to facilitate core cataloguing. During core sampling, reliable radioactive carbon isotope dating materials, such as carbon fragments and terrestrial plant residues, that were found in the core were dated using ^{14}C dating, and samples of quartz-rich sand-bearing layers in the core were dated using optically stimulated luminescence (OSL) (Sun, 2012; Tao, 2020).

To determine the age of the piedmont terrace, photoluminescent samples were taken from the sedimentary strata of the piedmont terrace. The sampling principle of light-emitting samples was strictly followed during the sampling, and the preservation in the later period was also ensured using a strip that completely blocked light. All OSL sample analyses were completed at the OSL Laboratory of the National Institute of Natural Hazards. Sediment photoluminescence dating can be expressed as follows: age (A) = equivalent dose (DE)/environmental dose rate (D). Pretreatment with test sample preparation at the Key Laboratory of Crustal Dynamics, China Earthquake Administration, National Institute of Natural Hazards, in a dark room under weak light involved opening the packing and removing the iron pipe ends that may have been exposed and retaining the centre without contamination. For the samples that were used to determine the equivalent dose of exposure, 20 g were taken to measure the moisture content and saturation coefficient. Then, dry grinding was performed. The contents of U, Th and K in the samples were determined after the samples passed through a 63 μm sieve. For the measurement of equivalent dose, the sample photoluminescent irradiation and signal were measured on the Danish Risoeda-20-C/D thermal/photoluminescent automatic measurement system of the Crustal Dynamics Laboratory of China Earthquake Administration. The natural photoluminescent dose (i.e., palaeodose) of the sample was measured by a monolithic reproduction method. For the environmental dose rate measurement, the ambient radiation dose absorbed by the sample was provided by the ionizing radiation generated by the alpha, beta and gamma decay of the radionuclides (238U, 232Th and 40K) in the sample itself and the surrounding sediments, with a small contribution from cosmic rays. The contents of U, Th and K in the samples were determined by element plasma mass spectrometry at the Beijing Research Institute of Uranium Geology. Finally, the age of the sample was calculated (Aitken, 1998; Murray and Wintle, 2003).

Since the development of the ^{14}C dating method, both theory and technology have matured from initial applications in archaeology to applications in geology (Qian, 2014; Zhao et al., 2017; Sanchez et al., 2018). The basic principle of the ^{14}C dating technique is to calculate the age of a sample according to the decay rate of ^{14}C atoms in the sample. Every living organism on Earth is involved in the exchange of carbon dioxide, and ^{14}C is present. Once an organism dies, there is no replacement of ^{14}C in the organism, and its original ^{14}C concentration decreases exponentially over time. During sample dating, the age of biological death is calculated based on the existing ^{14}C content of the sample to determine the age of the sample (Gao et al., 2004). Sample preparation methods were as follows: first, a proper amount of samples was taken, and roots, leaves and other plant residues and carbon fragments were selected. The second step was to put the selected loose samples into a 15 ml centrifuge tube and stir them with dilute sulfuric acid to remove inorganic carbonate. The third step was to add 2% Na OH solution to remove humic acid and clean the sample until neutral. The fourth step was to dry the sample at a constant temperature of 55°C and grind and wrap it for testing (Tao, 2020).

4 RESULTS

4.1 Fault Displacements and Slip Rates Along the Sertengshan Piedmont Fault

4.1.1 Piedmont Terrace Ages

The sedimentary strata of the Sertengshan piedmont terrace are mainly alluvial-diluvial sand and gravel layers and yellow–green lacustrine layers (**Figure 3D**). According to the dating data of the terrace strata, the age of the yellow–green lacustrine layer top is approximately 70 ka (**Figure 3B**). Chen et al. (2008) dated the top of the lacustrine layer in the HTS4 borehole to 71.90 ± 7.34 ka, which is similar to the dating results in this paper in the front terrace. As is apparent from **Supplementary Table S1**, the sedimentary age of the lacustrine layer in the T3 terrace is between 50 and 70 ka. The sedimentary age of the T2 terrace lacustrine layer is between 20 and 40 ka. The age of the T1 terrace sedimentary strata is approximately 10 ka, and the sedimentary strata are mainly interbedded with clay and gravel. The age of the clay layer on the T1 terrace in northeastern Wujiahe town is 9.29 ± 1.11 ka (**Figure 3A**). The sedimentary strata on the T1 terrace in northern Dongquanzicun are mainly composed of sand and gravel layers, and the two OSL ages are 8.32 ± 0.96 ka and 9.79 ± 1.44 ka. Moreover, several faults can be found in the outcrop. The faults may extend to the surface (**Figure 3C**). Liu et al. (2014) carried out OSL dating of sedimentary strata in the Hetao Basin through drilling. We used the QK3 borehole, which had complete stratigraphic ages, as the standard borehole for comparison. According to the selection basis of marker strata, the yellow–green lacustrine top was regarded as the marker strata, and the upper and lower stratigraphic sequences are completely different, with obvious characteristics. Therefore, the late Pleistocene slip rate could be calculated based on the displacement and age of the lacustrine strata, while the Holocene slip rate could be calculated based on the Holocene stratigraphic thickness and T1 terrace height within the basin.

4.1.2 Vertical Slip Displacement of the Sertengshan Piedmont Fault

The multistage activities of the Sertengshan piedmont fault resulted in the formation of a multistage terrace, and the height of each terrace reflects the uplift height of the footwall of the faults in different periods. According to the RTK measurement results, the height of terraces in front of Sertengshan was calculated in this

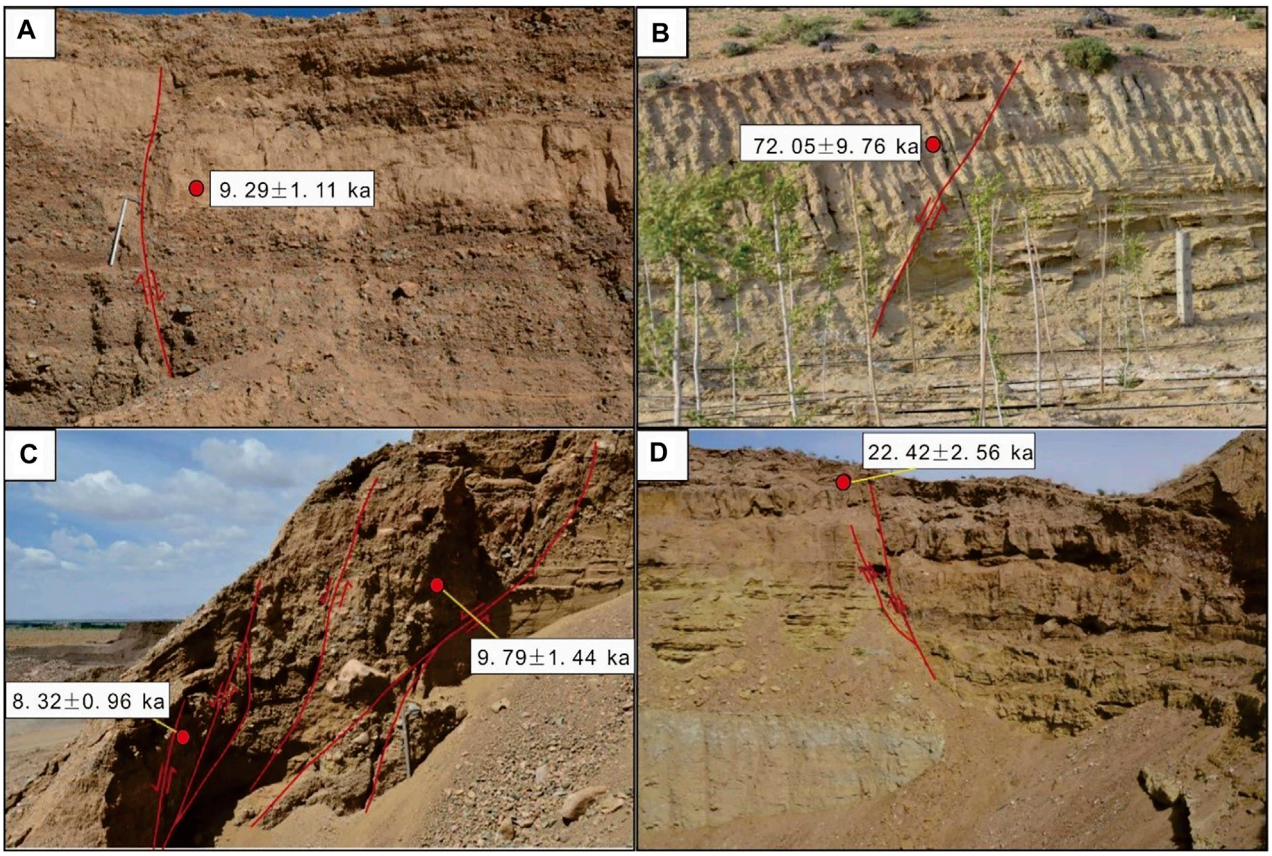

FIGURE 3 | Typical sampling points and ages in **(A)** northeastern Wujiahe town (looking SE); **(B)** Xiliuquanzixi (looking NW); **(C)** northern Dongquanzi (looking W); and **(D)** northeastern Dashetai town (looking SE).

paper. The results are shown in **Supplementary Table S2**. **Supplementary Figures S1–S3** show geological maps of the terraces associated with the Langshankou segment, Hongqicun segment and Kuluebulong segment.

As shown in **Supplementary Table S2**, the height of T1 terrace is approximately 7 m. Some of T1 terrace is relatively low because there are flood channels around it, and the height of terrace has been reduced due to flood erosion. The height of T2 terrace is approximately 14 m, the height of T3 terrace is approximately 26 m, and the height of T4 terrace is approximately 40 m. The Wujiahe segment and Hongqicun segment of the Sertengshan piedmont fault have more fourth-grade terraces and higher terraces, while the Kuluebulong segment and Dashetai segment have more developed third-grade terraces. Because the progression and height of the terrace can reflect the relative strength of activity of each segment, the activity of the Wujiahe and Hongqicun segments is the strongest, that of the Kuluebulong segment is weak, and that of the Dashetai segment is the weakest.

To obtain the displacement of the hanging wall, we used the borehole data of the Hetao Basin for comparative analysis. The stratigraphic age of the Hetao Basin is based on the age of QK3 (Liu et al., 2014). Boreholes VI-3 and QK3 are close to each other, so it can be considered that the sedimentary sequences of the two boreholes are similar. We describe the lithology of borehole VI-3 in **Supplementary Table S7**. According to the borehole lithologic profile, it can be found that the Holocene strata are gravel layer and clay sand layer, and the Holocene strata in VIII-1 and VIII-1 are mainly fine sand layer and clay sand layer, indicating that the sedimentary environment in this area is relatively stable. In the four boreholes Zh18, Zk3, Zk6 and Zk7, the Holocene strata are relatively fine, with sand and gravel layers in the middle, indicating that the formation was formed under the interaction of strong flowing water and static water environment. The strata of VI-1, H12 and H141 are all gravel beds since 65 ka in the late Pleistocene, indicating that these three places have strong activity and strong flowing water environment. Due to the inhomogeneity of the activity of piedmont fault zone in space, the elevation of the top of lacustrine layer in the borehole is different, and the thickness of sedimentary strata is different in different time periods. According to the lithologic characteristics of each borehole and the selection principle of marker strata, we select the top of silt layer, clay sand layer and yellow-green fine sand layer as the top of lacustrine layer (**Figure 4A**). The ancient, large Jilantai-Hetao lakes existed from 50 to 60 ka (Chen et al., 2008). According to the borehole data on the Hetao Basin, the age of the top of the lacustrine layer is approximately 65 ka.

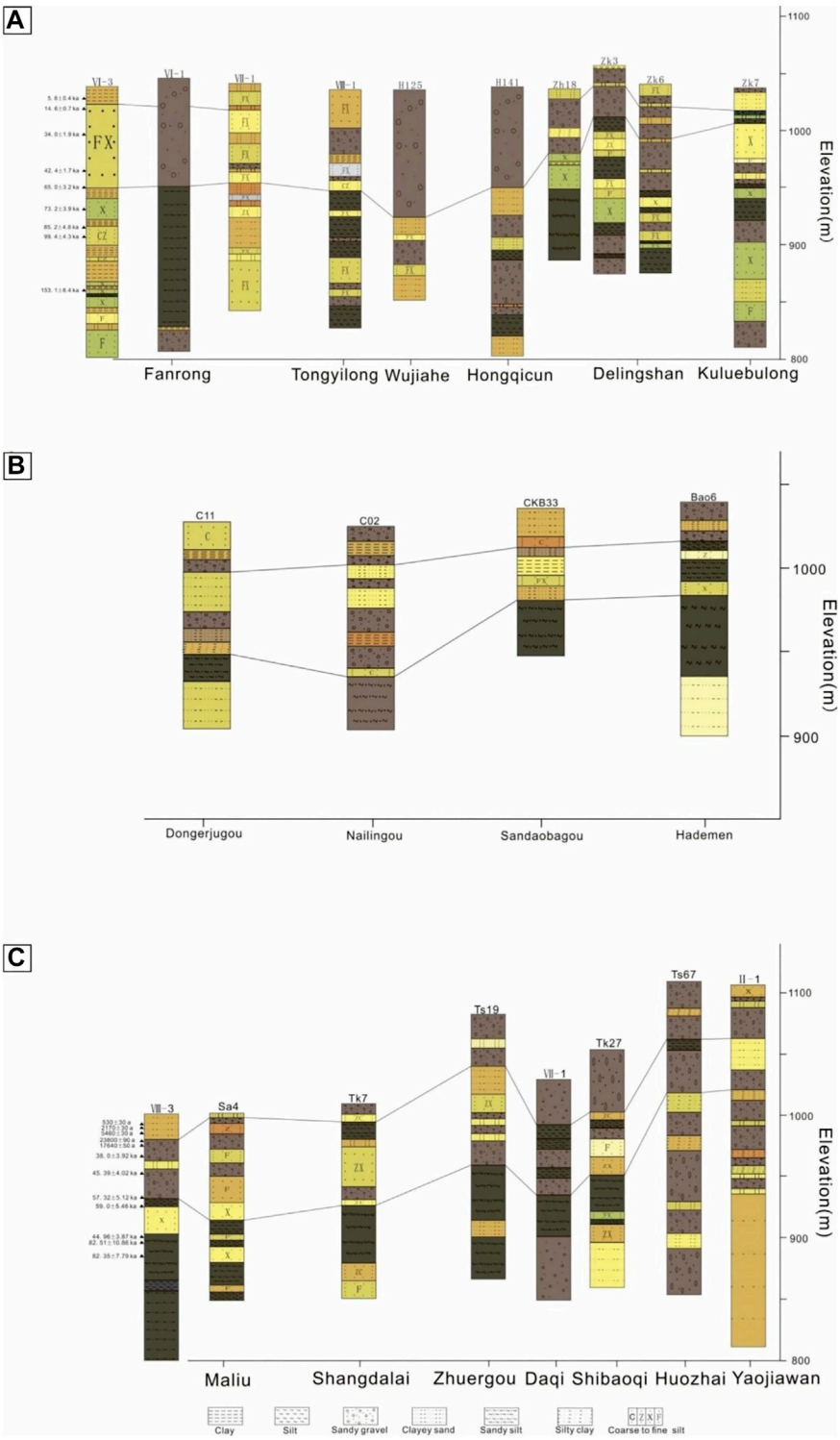

FIGURE 4 | (A) Column diagram of boreholes in front of Sertengshan; **(B)** Column diagram of boreholes in front of Wulashan; **(C)** Column diagram of boreholes in front of Daqingshan.

4.1.3 Slip Rate of the Sertengshan Piedmont Fault

According to the displacement calculation method, we used the above data from nine boreholes, combined with the RTK data and the measured terrace height, to calculate the displacement of the fault. **Figure 5A** shows the elevation distribution of the terraces and boreholes. Based on these data and the elevation of the 65.0 ± 3.2 ka

surface of the lacustrine layer top in the borehole, the displacement ranges of the Sertengshan piedmont fault since the late Pleistocene can be calculated for different places. The displacement was calibrated according to the distance L between the borehole and the terrace and the dip angle α of the marker strata.

Table 1 shows the displacement at the nine measuring points since 65.0 ± 3.2 ka in the late Pleistocene, and the displacement h of each measuring point is as follows: 113.7 m in Fanrong, 94.2 m in Fengyucun, 102.6 m in Tongyilong, 117.4 m in Wujiahe, 108.2 m in Hongqicun, 63.5 m in Wubulangkou, 57.6 m in northern Delingshan, 61.1 m in Xishuiquancun and 48.2 m in Kuluebulong. The average slip rates are 1.75 mm/a in Fanrong, 1.45 mm/a in Fengyucun, 1.58 mm/a in Tongyilong, 1.81 mm/a in Wujiahe, 1.66 mm/a in Hongqicun, 0.98 mm/a in Wubulangkou, 0.89 mm/a in northern Delingshan, 0.94 mm/a in Xishuiquancun, and 0.74 mm/a in Kuluebulong. The Fanrongcun measuring point is located at the westernmost end of the Sertengshan piedmont fault. According to the trend of fault activity, its slip rate should be low, but in fact, its slip rate is high, which may be related to its proximity to the Langshan piedmont fault.

The stratigraphic thickness since the start of the Holocene cannot be determined by the sedimentary strata in three boreholes (VIII-1, H125 and H141), which may lead to errors in the correlation of marker strata. In addition, the Holocene strata are mainly alluvial-diluvial strata, so it is impossible to correct the vertical displacement of the Holocene marker strata for all boreholes according to the dip angle of the strata. A borehole without correction of Holocene displacement gives the maximum displacement amplitude during the Holocene. **Table 1** lists the displacement ranges in the Holocene at six measuring points. The displacement at each measuring point is 17.7 m in Fanrongcun, 20.6 m in Fengyucun, 10.5 m in Wubulangkou, 24.4 m in northern Delingshan, 12.6 m in Xishuiquancun and 22.2 m in Kuluebulong. The corresponding average slip rates during the Holocene are 1.48 mm/a in Fanrongcun, 1.72 mm/a in Fengyucun, 0.86 mm/a in Wubulangkou, 2.03 mm/a in northern Delingshan, 1.05 mm/a in Xishuiquancun, and 1.85 mm/a in Kuluebulong. In the Tongyilong, Wujiahe and Hongqicun boreholes, the Holocene stratigraphic boundary cannot be clearly demarcated, but according to the slip rate since the late Pleistocene, the Holocene stratigraphic thickness is approximately 15 m in the Tongyilong, approximately 18 m in Wujiahe, and approximately 16 m in Hongqicun. Considering the elevation of the borehole and terrace, the average slip rates at Tongyilong, Wujiahe and Hongqicun during the Holocene are approximately 2.03, 2.28 and 1.86 mm/a, respectively.

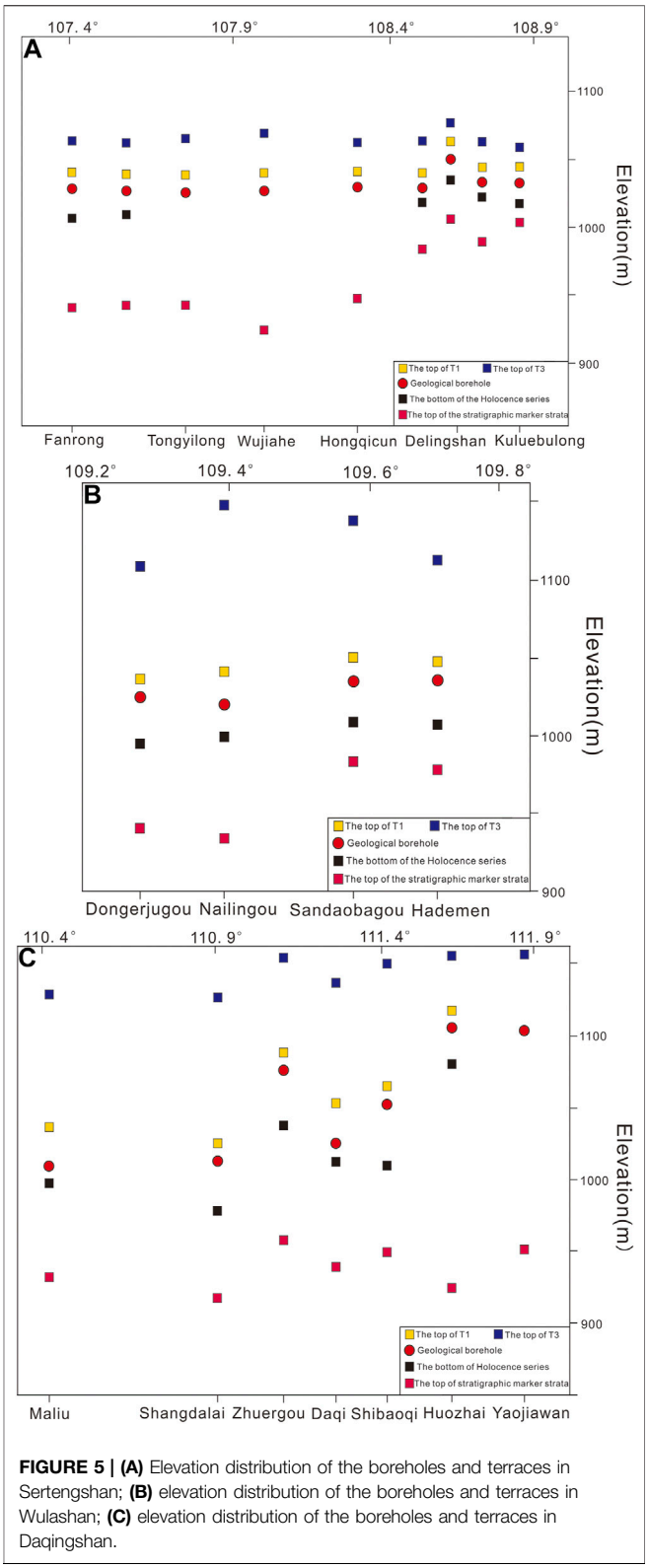

FIGURE 5 | (A) Elevation distribution of the boreholes and terraces in Sertengshan; **(B)** elevation distribution of the boreholes and terraces in Wulashan; **(C)** elevation distribution of the boreholes and terraces in Daqingshan.

4.2 Fault Displacements and Slip Rates Along the Wulashan Piedmont Fault

4.2.1 Elevations and Stratigraphic Ages of the Piedmont Terrace

To analyse the characteristics of the piedmont terrace of Wulashan, we conducted a field exploration (**Figure 6**). Due to the lack of data along the Wulateqianqi segment, we summarized the elevations and ages of terraces around the other two segments. Among them, the T1 terrace from Gongmiaozi to Heshunzhuang is not well developed, the yellow–green sand layer with horizontal bedding is exposed on the front edge of the terrace in some sections, and the elevation of

TABLE 1 | Vertical displacement of the Sertengshan piedmont fault.

Location	Fanrong	Fengyu	Tongyilong	Wujiahe	Hongqicun	Wubulangkou	Delingshan	Xishuiquan	Kuluebulong
Borehole	VI-1	VII-1	VIII-1	H125	H141	ZH18	ZK3	ZK6	ZK7
T3 elevation (m)	1,062.5	1,060.4	1,063.0	1,064.0	1,060.0	1,061.0	1,068.0	1,060.0	1,058.0
T1 elevation (m)	1,042.5	1,042.0	1,045.0	1,045.5	1,043.3	1,041.0	1,061.0	1,043.2	1,043.0
Wellhead elevation (m)	1,040.6	1,036.2	1,035.6	1,036.1	1,037.0	1,037.3	1,055.7	1,039.8	1,036.4
Elevation of the Holocene series in the footwall (m)	1,017.9	1,021.4	—	—	—	1,030.5	1,035.2	1,026.2	1,018.2
Vertical displacement of the Holocene series (m)	24.6	20.6	—	—	—	10.5	25.8	17.0	24.8
Holocene vertical displacement after correction (m)	17.7	—	—	—	—	—	24.4	12.6	22.2
Elevation of the top of the lacustrine strata (m)	941.9	942.3	942.6	925.0	947.6	984.1	1,009.0	994.5	1,007.2
Displacement of the stratigraphic marker strata since 65 ka (m)	120.6	118.1	120.4	139.0	112.4	76.9	59.0	65.5	50.8
Vertical displacement after correction (m)	113.7	94.2	102.6	117.4	108.2	63.5	57.6	61.1	48.2

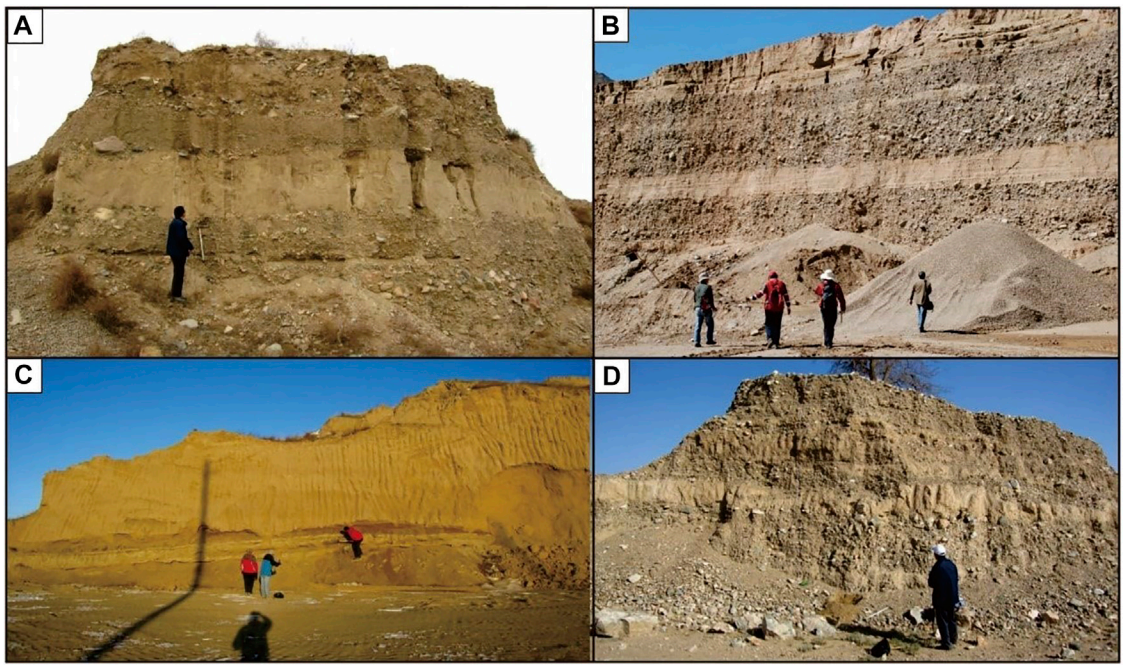

FIGURE 6 | (A) Holocene stratigraphic section in Shaota (NW), **(B)** Hademengou diluvial fan stratigraphic section, **(C)** East Kundulun River stratigraphic section (NE), and **(D)** Huhe Braggol Holocene stratigraphic section.

the terrace is 1,022–1,035 m. T2 is a pedestal terrace with granite gneisses in the basement and fluvial and lacustrine conglomerate in the upper part. It forms a continuous belt along the Wulashan piedmont fault with an elevation of 1,060–1,100 m. The T3 terrace is distributed intermittently in front of Wulashan, and the elevation is approximately 1,135 m. (dos Massif, 1988; Institute of Crustal and Dynamics and China Earthquake Administration, 2013; Research Group of Active Fault System around Or).

There have been many studies on the formation age of the terrace (**Supplementary Table S3**). Based on the analysis of the dating results of the samples collected in this work, we preliminarily determined that the formation age of the T1 terrace was the early Holocene, approximately 7–12 ka; the T2 terrace formed in the late Pleistocene, approximately 30–40 ka; and the T3 terrace formed in the middle of the latest Pleistocene, approximately 50–60 ka (He et al., 2020).

4.2.2 Vertical Slip Displacement of the Wulashan Piedmont Fault

To accurately determine the relative heights of the terraces, large-scale topographic maps of Xishanzui, Gongmiaozi, Dalagou, Meigeng, Hayehutong, Hademen and other places were produced with GPS RTK. The relative heights of various terraces along the

Wulashan piedmont fault are listed in **Supplementary Table S4**. **Supplementary Figures S5–S7** show the topographic maps and terrace data around Heshunzhuang, Hayehuutong and Dabagou.

To calculate the vertical displacement amplitude at each fault point, in this paper, large-scale GPS RTK-based topographic maps and borehole locations were used to estimate the corresponding elevations of T1 and T3 in Dongerjugou, Nailinggou, Santaobagou and Hademen. The results show that the elevations of T1 and T3 in Dongerjugou are 1,028.6 and 1,114.5 m, respectively. The elevations of T1 and T3 in Nailinggou are 1,040 and 1,150 m, respectively. In Sandaobagou, the elevation of T1 is 1,050 m, and the elevation of T3 is 1,140 m. In Hademen, the elevation of T1 is 1,045 m, and that of T3 is 1,120 m.

To obtain the displacement of the Wulashan piedmont fault, four boreholes in the hanging wall of the fault are used for comparative analysis (**Figure 4B**). According to **Figure 4B**, the Holocene strata in the four boreholes are mainly gravel, coarse sand, clay and clay sand. The Bao6 borehole is mainly sand and gravel layer, indicating that the sedimentary environment of the borehole is strong flowing water. The clay layer in C11 and C02 is overlying the sand and gravel layer, which indicates that the sedimentary environment tends to be stable in this period. The coarse sand layer and gravel layer in the uppermost layer are the result of alluviation. The Holocene strata of CKB33 are mainly coarse sand and clay sand, indicating that the sedimentary environment is relatively stable. The top of lacustrine layer of the four boreholes is the top of silt and sandy silt layer, with an elevation of 900–1000 m, which is close to the top of lacustrine layer of the boreholes in Daqingshan and Sertengshan. A great deal of work has been performed to date the terrace in front of Wulashan; the age of the T1 terrace is approximately 10–12 ka, and that of the T3 terrace is approximately 60 ka. According to the analysis of the piedmont boreholes in Daqingshan and Sertengshan, the ages of the top of the lacustrine layer are 65 ± 3.2 ka and 57.32 ± 5.12 ka, respectively, which are in the same period. Although the borehole on the hanging wall of the fault lacks chronological information, it belongs to the northern margin of the Hetao fault system and is located on the northern margin of the ancient lake. Therefore, it can be inferred that the age of the top of the lacustrine layer in the borehole on the southern side of the Wulashan piedmont fault is approximately 60 ka.

4.2.3 Slip Rate of the Wulashan Piedmont Fault

Figure 5B shows the elevation distribution of the terrace and borehole. Based on the elevation of the T3 terrace and the lacustrine layer in the borehole, the displacement of each measuring point can be calculated since the late Pleistocene. The displacement was calibrated according to the distance L between the borehole and the terrace and the dip angle α of the marker strata (**Table 2**).

Table 2 shows the displacement at four measuring points in the latest Pleistocene. Since the latest Pleistocene (60 ka), the displacement h at each measuring point is as follows: 145.3 m in Dongerjugou, 186.8 m in Nailinggou, 153 m in Sandaobagou and 128.24 m in Hademen. The corresponding average slip rates are 2.42 mm/a in Dongerjugou, 3.11/a in Nailinggou, 2.55/a in Sandaobagou and 2.14 mm/a in Hademen. Dongerjugou is located in the Gongmiaozi segment. In western Dongerjugou, the slip rate cannot be calculated due to the lack of borehole data. Analysis of the Heshunzhuang-Baotou segment shows that the fault slip rate has been decreasing from west to east since the late Pleistocene (60 ka).

Similar to the Holocene strata near Sertengshan, the Holocene strata in the basin on the southern side of Wulashan are mainly alluvial and diluvial. However, the Holocene strata in the borehole are easy to distinguish, so the displacement of Holocene marker strata can be corrected. The displacements at the four Holocene measuring points in **Table 2** are 21.5 m in Dongerjugou, 29.5 m in Nailinggou, 34 m in Sandaobagou and 22.4 m in Hademen. The corresponding Holocene slip rates are 1.84 mm/a in Dongerjugou, 2.52 mm/a in Nailinggou, 2.91 mm/a in Sandaobagou, and 1.91 mm/a in Hademen. Different from the late Pleistocene slip rate, the Holocene slip rate increases from west to east, but the slip rate is relatively small. The activity of the Wulashan piedmont fault since the late Pleistocene is stronger than that during the Holocene.

4.3 Fault Displacements and Slip Rates Along the Daqingshan Piedmont Fault

4.3.1 Vertical Slip Displacement of the Daqingshan Piedmont Fault

Since the late Pleistocene, the Daqingshan piedmont fault has formed three stages of terraces in the piedmont. The T1 terrace is an accumulative terrace, and the front of the terrace is a Holocene fault scarp. The T2 and T3 terraces are pedestal terraces (The Institute of Crustal and Dynamics and China Earthquake Administration, 1994) carried out research, including 1:50000 geological mapping, on the active Daqingshan piedmont fault and collected thermoluminescence (TL) age samples to determine the formation age of the terrace. The dating results suggest that the formation age of the T3 terrace was late Pleistocene. The age of the T1 terrace is approximately 11 ka, indicating Holocene formation. Therefore, the elevations of the T3 terrace and T1 terrace of the Daqingshan piedmont fault were used as marker elevations to calculate the vertical displacement of the Daqingshan piedmont fault in the late Pleistocene and Holocene.

In this paper, according to the measurement results of previous studies, the elevations of the T1 and T3 terraces in the Daqingshan piedmont fault were collected, and the results are shown in **Supplementary Table S5**.

As shown in **Supplementary Table S5**, the T3 terrace is continuously distributed along the Daqingshan piedmont fault and is largely complete. The relationship between the T2 and T3 terraces is erosional, and the development is discontinuous along the front of Daqingshan. T1 terraces are relatively well developed in the western segment of Tuyouqi and the western segment of Tuzuoqi, but the T1 and T2 terraces are not well developed in eastern Bikeqi.

To obtain the elevation of the maker strata in the hanging wall, we used boreholes in the Hetao Basin to carry out a comparative analysis. Because borehole VIII-3 is close to ZK2, it can be considered that the sedimentary sequences of the two boreholes are similar. **Supplementary Table S21** shows the

TABLE 2 | Vertical displacement of the Wulashan piedmont fault.

Location	Dongerjugou	Nailingou	Sandaobagou	Hademen
Borehole	C11	C02	CKB33	Bao6
T3 elevation (m)	1,114.5	1,150	1,140	1,120
T1 elevation (m)	1,028.5	1,040	1,050	1,045
Wellhead elevation (m)	1,026.1	1,024.4	1,036.9	1,040.9
Elevation of the Holocene series in the footwall (m)	998	1,005	1,014	1,011
Vertical displacement of the Holocene series (m)	30.5	35	36	34
Holocene vertical displacement after correction (m)	21.5	29.5	34	22.4
Elevation of the top of the lacustrine strata (m)	947	935	985	980
Displacement of the stratigraphic marker strata since 65 ka (m)	167.5	215	155	140
Vertical displacement after correction (m)	145.3	186.8	153	128.24

lithology of borehole VIII-3. **Supplementary Figure S7** shows field photographs and a lithologic histogram for borehole ZK2. **Figure 4C** shows 7 borehole lithologic profiles of Daqingshan piedmont fault. The Holocene strata in Sa4 are mainly sandy clay layers, indicating that the sedimentary environment is relatively stable. The Holocene strata in the five boreholes Tk7, Ts19, Ⅷ-1, Tk27 and TS67 are mainly gravel and middle coarse sand, with large grain size, indicating that they were formed under the action of strong water flow. The upper part of the Ⅱ-1 is composed of fine sand and silty clay, and the lower part of it is composed of sand and gravel, indicating that the sedimentary environment in the late Holocene was relatively stable after the strong flowing water. The top of lacustrine layer from Sa4 to Zk27 is silt layer or sandy silt layer. The top of yellow-green sand layer is selected as the top of lacustrine layer in Ts67 and Ⅱ-1.

The ages from borehole ZK2 were adopted. The age of the top of the lacustrine layer is approximately 58 ka, and the age of the bottom of the Holocene layer is approximately 11 ka.

4.3.2 Slip Rate of the Daqingshan Piedmont Fault

Figure 5C shows the elevation distribution of the terrace and borehole at 7 measuring points, and the displacement h at each measuring point since the late Pleistocene (57.32 ± 5.12 ka) is as follows: 195.21 m in Maliu, 145 m in Shangdalai, 186 m in Zhuergou, 187.98 m in Daqi, 188.15 m Shibaoqi, 225 m in Huozhai and 198.89 m in Yaojiawan (**Table 3**). The corresponding average slip rates are as follows: 3.37 mm/a in Maliu, 2.50 mm/a in Shangdalai, 3.21 mm/a in Zhuergou, 3.24 mm/a in Daqi, 3.25 mm/a in Shibaiqi, 3.88 mm/a in Huozhai, and 3.43 mm/a in Yaojiawan. Due to the lack of borehole data in the Baotou segment of the Daqingshan piedmont fault, the vertical slip rate has not been measured. However, according to the slip rates measured at seven measuring points, the average slip rate of the Daqingshan piedmont fault has no obvious regularity in terms of spatial distribution. Wu et al. (1996) calculated the average slip rates along the Baotou segment of the Daqingshan piedmont fault, with those in Wudangou (4.49 mm/a) and Wanshuiquan (2.61 mm/a) being consistent with those in this study.

The Holocene strata in the borehole are easy to distinguish, so the displacement of Holocene marker strata can be corrected. Due to the lack of the T1 terrace in the Hohhot segment of the Daqingshan piedmont fault, the vertical displacement cannot be calculated. Therefore, we use only six measuring points to calculate the Holocene vertical displacement. The h at each measuring point is as follows: 26.21 m in Maliu, 31 m in Shangdalai, 27 m in Zhuergou, 19.58 m in Daqi, 31.15 m in Shibaoqi and 27 m in Huozhai. The corresponding average slip rates are 2.37 mm/a in Maliu, 2.82 mm/a in Shangdalai, 2.45 mm/a in Zhuergou, 1.78 mm/a in Daqi, 2.83 mm/a in Shibaoqi, and 2.45 mm/a in Huozhai.

5 DISCUSSION

5.1 Interpretation of Fault Slip Rate and Revelation of Seismic Hazard Along the Northern Margin of the Hetao Basin

Much work has been conducted on the slip rates of faults along the northern margin of the Hetao Basin. However, the calculation of fault slip in this region has been simplified. In the 1990s, the state seismological bureau organized the study entitled "1:50000 Geological Mapping and Comprehensive Research of Langshan-Sertengshan Piedmont Fault." For the Sertengshan piedmont fault, the calculated maximum slip rate since the late Pleistocene was 3.6 mm/a, and the calculated slip rate during the Holocene was 2.2 mm/a (Institute of Crustal and Dynamics and China Earthquake Administration, 1994). Ma et al. (1998) divided the piedmont terrace of Wulashan into high terrace and low terrace areas. They believed that the relative height of the high terrace areas represents the uplift displacement of the fault since the late Pleistocene and that of the low terrace areas represents the uplift displacement of the fault during the Holocene. Based on the relative height and thermoluminescence dating data of the high and low terraces, the uplift rate of the fault footwall is 0.5–2 mm/a since the late Pleistocene and 0.4–1.0 mm/a during the Holocene. Wu et al. (1996) obtained the displacement of the fault in the latest Pleistocene by comparing the footwall terrace of the Daqingshan piedmont fault with the corresponding marker strata in a borehole in the hanging wall; they then obtained the corrected displacement as the vertical displacement of the fault according to the dip angle of the marker strata. According to the thermoluminescence age data of the terrace, the vertical slip rate of the fault since the latest Pleistocene is 2.61–4.49 mm/a. To approximate the Holocene displacement, the free-face ratio of height to the distance between the upper and lower fault scarps is calculated, and the vertical slip rate of the fault during the

TABLE 3 | Vertical displacement of the Daqingshan piedmont fault.

Location	Maliu	Shangdalai	Zhuergou	Daqi	Shibaoqi	Huozhai	Yaojiawan
Borehole	Sa4	TK7	TS19	VII-1	TK27	TS67	II-1
T3 elevation (m)	1,128	1,120	1,154	1,143	1,150	1,155	1,170
T1 elevation (m)	1,039	1,056	1,083	1,052	1,058	1,112	
Wellhead elevation (m)	1,014.1	1,011	1,078	1,030.7	1,054.4	1,109.7	1,108.21
Elevation of the Holocene series in the footwall (m)	1,008	980	1,048	1,020	1,015	1,080	—
Vertical displacement of the Holocene series (m)	31	76	35	32	43	32	—
Holocene vertical displacement after correction (m)	26.21	31	27	19.58	31.15	27	—
Elevation of the top of the lacustrine strata (m)	928	930	960	942.6	950	925	952.21
Displacement of the stratigraphic marker strata since 65 ka (m)	200	190	194	200.4	200	230	217.79
Vertical displacement after correction (m)	195.21	145	186	187.98	188.15	225	198.89

Holocene is 0.37–1.72 mm/a. The Langshan piedmont fault is located on the northwestern margin of the Hetao Basin. Much work has been conducted on the fault activity of the Langshan piedmont fault. The fault dislocated the bottom layer of the Holocene and forced the Yellow River to migrate southward in modern times, with a vertical slip rate of 0.47–2.2 mm/a in the Holocene (Sun et al., 1990; Deng et al., 1999). He et al. (2014) inferred that the uplift rate since 47.4 ka was 0.81–1.8 mm/a by studying typical profiles of terraces along the Langshan piedmont fault. He et al. (2015) conducted a systematic study on ten debris flow gullies in the central and southern parts of the region, combined with an assessment of tectonic movement, and concluded that the uplift rate of the middle segment of the Langshan piedmont fault was 2.8 mm/a. (Dong, 2015) excavated multiple trenches in the Langshan piedmont fault and concluded that the vertical slip rate of Qingshan town was 1.33–1.44 mm/a in the Holocene. However, we believe that the vertical slip rate estimated based on the dislocation of the same strata in trenches or terrace elevations are not representative of the entire fault, and the calculated rate is too small. Liang (2019) re-estimated the vertical slip rate of the Langshan piedmont fault since the late Pleistocene based on the throw between the top of the same lacustrine strata on both sides of the fault and concluded that the vertical slip rate of the Langshan piedmont fault since the late Pleistocene was 1.8–3.2 mm/a, which is more accurate.

In previous studies of the fault slip rate on the northern margin of the Hetao Basin, calculations were mostly based on the uplift rate of the faults. In addition, the calculation of the fault uplift rate by directly using terrace height and age without considering the influence of terrace sedimentary cover will lead to inaccurate results. Moreover, due to the limitations of dating technology, thermoluminescence dating is the most common method to obtain age estimates. The dating accuracy of this method is lower than that of OSL dating. These limitations lead to the underestimation of fault activity and earthquake risk. Most previous studies calculated the slip rates of faults by the cumulative dislocation of palaeoseismic events in profiles and troughs but did not consider the creep slip rate of faults between ruptured earthquakes. Studies have shown that long-term deformation monitoring across faults using high-precision measurement arrays, such as short-range leveling, short baseline and creep meter surveys, is an effective method for obtaining the current activity mode and behaviour of faults (Savage et al., 1979; Bevis and Isacks, 1981; Lisowski and Prescott, 1981; Schulz et al., 1982; Lee et al., 2001; Lienkaemper et al., 2001,2013, 2014; Du et al., 2010; Zhang et al., 2018). Yang et al. (2021) analysed the activity of the Kouzhen-Guanshan fault in the Weihe Basin from the late Quaternary to the present based on field investigation results and cross-fault deformation data and concluded that the vertical creep rate of the eastern segment of the fault is 1.56 mm/a, suggesting that a long period of cross-fault deformation monitoring is needed to thoroughly study the activity of a fault. The Hetao Basin and Weihe Basin in this study area both fault-controlled basins around the Ordos block, and their fault activity models are similar. Therefore, we believe that the vertical slip rates of these normal faults constrained by terraces and boreholes consist of both seismic stick-slip and interseismic creep slip rates. Considering the monitoring data of cross-fault deformation in the study area, we will further study the fault creep rates of the faults in the future.

The vertical displacement calculated in this paper by using the marker strata of the borehole and terrace can represent the real displacement of the fault and is not affected by the surface sediment cover. Therefore, the calculated vertical slip rate is the complete vertical slip rate of the fault, which can provide support for evaluating the seismic hazard of the fault. In addition, the vertical slip rates obtained in this paper include the interseismic creep slip rates of the faults, which will be further studied.

Table 4 shows that since 65 ka in the late Pleistocene, the average slip rates of the three segments of the Sertengshan piedmont fault are 1.65 mm/a in the Langshankou segment, 1.32 mm/a in the Hongqicun segment and 0.86 mm/a in the Kuluebulong segment, showing a decreasing trend from west to east. Since the late Pleistocene (60 ka), the average slip rates of the two segments of the Wulashan piedmont fault have been 2.42 mm/a in the Gongmiaozi segment and 2.6 mm/a in the eastern Baotou segment. The average slip rates of the segments show an increasing trend from west to east. Since the late Pleistocene (58 ka), the average slip rates of the four segments of the Daqingshan piedmont fault are as follows: 3.37 mm/a in the Tuyouxi segment, 2.50 mm/a in the Tuzuoxi segment, 3.40 mm/a in the Bikeqi segment and 3.43 mm/a in the Hohhot segment. Among them, the average slip rate in the Bikeqi segment is the highest, and that in the Tuzuoqi segment is the lowest. Moreover, the maximum and minimum slip rates at each measuring point also appear in the Bikeqi segment and the Tuzuoxi segment, respectively. The vertical slip rate at each measuring point in the Bikeqi segment presents an increasing trend

TABLE 4 | Comparison of late Pleistocene slip rates of active faults on the northern margin of the Hetao Basin.

Name of the fault	Segment	Measuring point	Vertical slip rate at the point	Average slip rate of the segment	Average slip rate of the fault
Sertengshan piedmont fault	Langshankou segment	Fanrong	1.75	1.65	1.28
		Fengyu	1.45		
		Tongyilong	1.58		
		Wujiahe	1.81		
	Hongqicun segment	Hongqicun	1.66	1.32	
		Wubulangkou	0.98		
	Kuluebulong segment	Delingshan	0.89	0.86	
		Xishuiquan	0.94		
		Kuluebulong	0.74		
Wulashan piedmont fault	Gongmiaozi segment	Dongerjugou	2.42	2.42	2.51
	Baotou segment	Nailingou	3.11	2.6	
		Sandaobagou	2.55		
		Hademen	2.14		
Daqingshan piedmont fault	Tuyouxi segment	Maliu	3.37	3.37	3.34
	Tuzuoxi segment	Shangdalai	2.50	2.50	
	Bikeqi segment	Zhuergou	3.21	3.40	
		Daqi	3.24		
		Shibaoqi	3.25		
		Huozhai	3.88		
	Hohhot segment	Yaojiawan	3.43	3.43	

from west to east. By comparing the average slip rates of the three faults since the late Pleistocene, it can be found that the average slip rate of the Daqingshan piedmont fault is the highest (3.34 mm/a), and the average slip rate of the Sertengshan piedmont fault is the lowest (1.28 mm/a). According to the spatial distribution of the three faults on the northern margin of the Hetao Basin, the activity of the three active faults increases from west to east.

Table 5 shows that since 12 ka, the average slip rates of the three segments of the Sertengshan piedmont fault are 1.88 mm/a (Langshankou segment), 1.36 mm/a (Hongqicun segment) and 1.64 mm/a (Kuluebulong segment), showing no obvious spatial pattern. The average slip rates of the two segments of the Wulashan piedmont fault are 1.84 mm/a in Gongmiaozi and 2.45 mm/a in Baotou, showing an increase from west to east. Since 11 ka, the average slip rates of the three segments of the Daqingshan piedmont fault are 2.37 mm/a in the Tuyouxi segment, 2.82 mm/a in the Tuzuoxi segment and 2.38 mm/a in the Bikeqi segment. The average slip rate of each segment increases from west to east. By comparing the average slip rates of three active faults on the northern margin of the Hetao Basin, it can be found that since the Holocene, the average slip rate of the Daqingshan piedmont fault is the highest (2.45 mm/a), and that of the Sertengshan piedmont fault is the lowest (1.68 mm/a). Similar to that during the late Pleistocene, the activity of the three faults during the Holocene increases from west to east.

By comparing **Tables 4**, **5**, it can be found that the average slip rate of each segment of the Sertengshan piedmont fault since the late Pleistocene is less than that during the Holocene; that is, the fault activity of the Sertengshan piedmont fault increased from the late Pleistocene to the Holocene. The average slip rates of the Daqingshan piedmont fault and Wulashan piedmont fault since the late Pleistocene are greater than those during the Holocene; that is, the fault activity of the Daqingshan piedmont fault and Wulashan piedmont fault decreased from the late Pleistocene to the Holocene.

Table 6 summarizes the elapsed time and mean recurrence interval of the last palaeoseismic event of the main active fault segments in the Hetao fault zone. By consulting the recurrence characteristics of palaeoearthquakes and the vertical slip rates obtained in this paper, it can be found that in the Langshankou and Hongqicun segments of the Sertengshan piedmont fault, the elapsed time since the latest earthquake is close to or longer than the recurrence interval and that the activity of the fault segments increased from the late Pleistocene to the Holocene, suggesting that the future seismic risk of the two fault segments is high. In contrast, the elapsed times of the Kuluebulong and Dashetai segments are less than the average recurrence interval, and the late Pleistocene-Holocene fault segments are not currently active, so we can conclude that the Kuluebulong and Dashetai segments will have low earthquake risk in the future. It is difficult to estimate the seismic risk along the Wulateqianqi segment of the Wulashan piedmont fault because of the lack of a complete palaeoearthquake sequence and earthquake recurrence interval. However, the elapsed time since the last palaeoearthquake in the Baotou segment is close to the average recurrence interval, and the slip rate is high, so the possibility of future earthquakes is high. In addition, the elapsed time since the last palaeoearthquake in the Gongmiaozi segment is far less than the average recurrence interval, and the slip rate of the fault segment is not high, so the risk of future earthquakes is low. Among the fault segments of the Daqingshan piedmont fault, the characteristic earthquake recurrence interval and slip rate of the Baotou segment were not obtained, so it is difficult to estimate the seismic risk for this segment. Although the elapsed time since the latest palaeoearthquake in the Tuyouxi segment is less than the recurrence interval, the slip rate of this fault section is high, so the seismic risk of this segment cannot be ignored. In addition, the

TABLE 5 | Comparison of the Holocene slip rates of active faults on the northern margin of the Hetao Basin.

Name of the fault	Segment	Measuring point	Vertical slip rate at the point	Average slip rate of the segment	Average slip rate of the fault
Sertengshan piedmont fault	Langshankou segment	Fanrong	1.48	1.88	1.68
		Fengyu	1.72		
		Tongyilong	2.03		
		Wujiahe	2.28		
	Hongqicun segment	Hongqicun	1.86	1.36	
		Wubulangkou	0.86		
	Kuluebulong segment	Delingshan	2.03	1.64	
		Xishuiquan	1.05		
		Kuluebulong	1.85		
Wulashan piedmont fault	Gongmiaozi segment	Dongerjugou	1.84	1.84	2.30
	Baotou segment	Nailingou	2.52	2.45	
		Sandaobagou	2.91		
		Hademen	1.91		
Daqingshan piedmont fault	Tuyouxi segment	Maliu	2.37	2.37	2.45
	Tuzuoxi segment	Shangdalai	2.82	2.82	
	Bikeqi segment	Zhuergou	2.45	2.38	
		Daqi	1.78		
		Shibaoqi	2.83		
		Huozhai	2.45		
	Hohhot segment	Yaojiawan	—		

TABLE 6 | The elapsed time since the last palaeoseismic event and mean earthquake recurrence interval for segments along the northern margin of the Hetao Basin.

Name of the fault	Segment	Elapsed time (a B.P.)	Mean recurrence interval (a)	Data source
Sertengshan piedmont fault	Langshankou segment	4190 ± 250	4125	Chen (2002)
	Hongqicun segment	3250 ± 250	4105	Chen (2002)
	Kuluebulong segment	2320	4105	Zhang (2017)
	Dashetai segment	3590	4093	He et al. (2018)
Wulashan piedmont fault	Wulateqianqi segment	<17000		Previous study[a]
	Gongmiaozi segment	1655 ± 185	8533	Ran et al. (2003)
	Baotou segment	4130 ± 78	4314	Chen (2002)
Daqingshan piedmont fault	Baotou segment	3390 ± 2140		Ran et al. (2003)
	Tuyouxi segment	1165	1788	He and Ma (2015)
	Tuzuoxi segment	>10,790	2948 ± 560	Ran et al. (2003)
	Bikeqi segment	2867 ± 679	2763 ± 518	He (2006)
	Hohhot segment	4500 ± 230	2642 ± 412	He (2006)

[a]*Institute of Crustal and Dynamics and China Earthquake Administration (2013).*

elapsed times since the last palaeoearthquake in the Tuzuoxi, Bikeqi and Hohhot segments are longer than the average recurrence intervals, and the slip rates of those fault segments are high; thus, we conclude that these three segments have high seismic risk.

5.2 Fault Slip Rate and Regional Tectonic Dynamics Along the Northern Margin of the Hetao Basin

The faulted basins around the Ordos block are considered to be the common result of the westward subduction of the Pacific plate and the collision between the Indian plate and Eurasian plate (Liu et al., 2004; Northrup et al., 1995; Tian et al., 1992; Xu et al., 2019). The sedimentary-tectonic evolution history of Cenozoic faulted basins around the Ordos block and the shift in tensile stress direction clearly record the remote effects of the convergence of different plates and deep tectonothermal activity (Shi et al., 2020; Zhang et al., 2006; Zhu et al., 2012). Zhang et al. (2019) stated that the remote effect of the Indo-Eurasian plate collision and deep mantle upwelling induced by Pacific subduction interacted in North China and jointly drove the extensional deformation around the Ordos block. Deng et al. (1999) proposed a dynamic model of the formation and evolution of the Ordos block and its adjacent fault basins. They concluded that several late Mesozoic to early Cenozoic uplift belts around the Ordos block developed under NE-ENE compression of the Tibetan Plateau. On the axis of these uplifts, the upper crust was subjected to secondary tensile stress, easily resulting in ruptures. Once positive strike-slip faults or normal faults began to occur along the rupture, they gradually controlled the development of a series of fault basins. Thus, a discontinuous shear-extensional fault basin belt composed of multiple graben or half-graben basins formed. Furthermore, isostatic adjustment occurred once a faulted basin or faulted basin

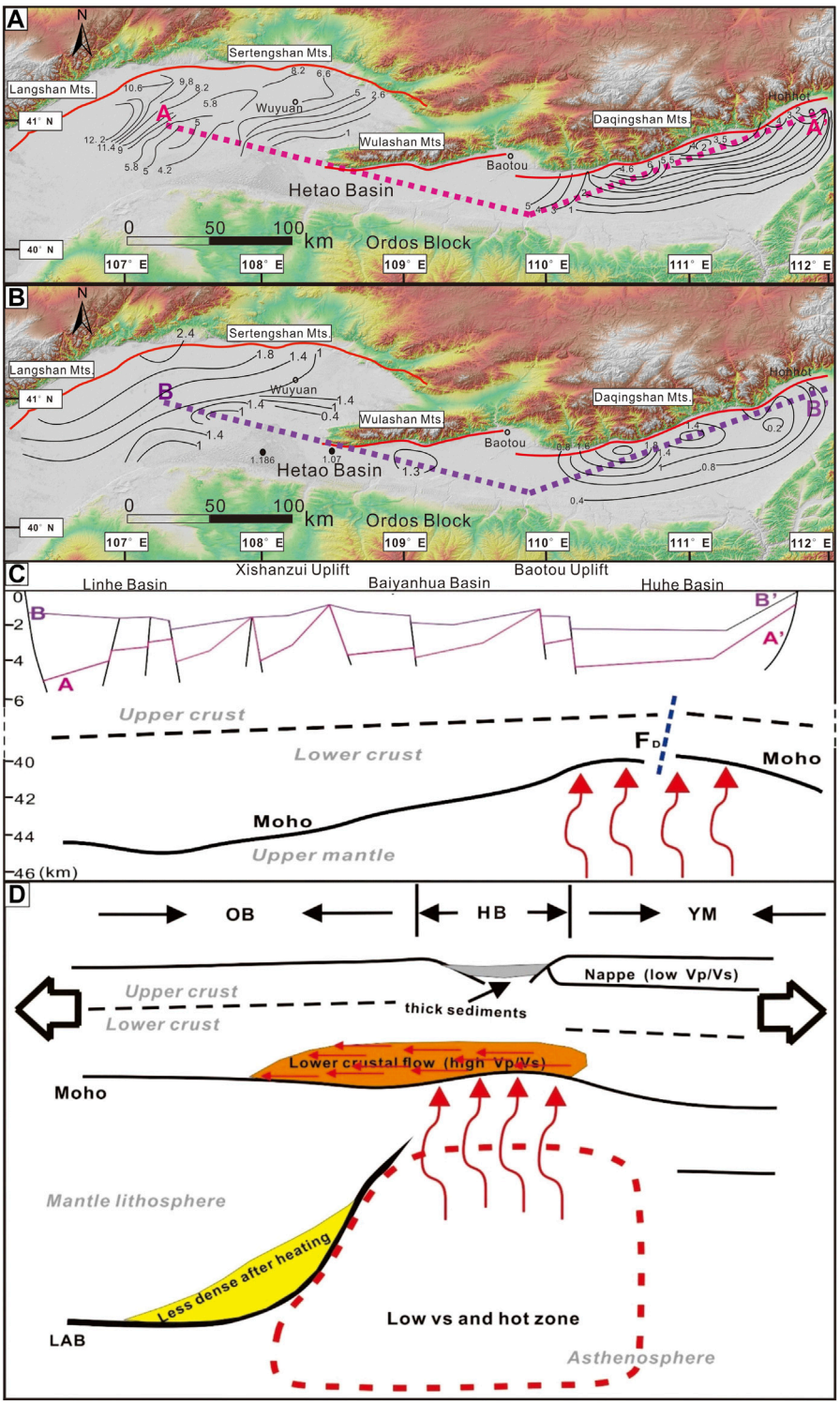

FIGURE 7 | (A) Cenozoic floor isopath (km), thickness from (Li and Nie, 1987); **(B)** Quaternary floor isopach (km), thickness from (Research Group of Active Fault System around Ordos Massif, 1988); **(C)** AA′, Cenozoic floor isopach profile in the Hetao Basin; BB′, Quaternary isopach profile in the Hetao basin. The FD is the deep fault below Daqingshan (Feng et al., 2015). The red arrow represents the upwelling of deep material below the fracture. The Moho surface depth comes from (Feng et al., 2015) **(D)** Dynamic processes beneath the study area (modified from Teng et al., 2010); OB, Ordos block; HB, Hetao Basin; YM, Yinshan Mountains. The dotted line is the upper and lower crustal boundary of the WRR structure (Teng et al., 2010). LAB represents the lithosphere-asthenosphere boundary, and its depth comes from (Chen et al., 2009; Huang et al., 2009). The region surrounded by the red dotted line represents the lower V region and heat region of the upper mantle; the red arrow

(*Continued*)

FIGURE 7 | represents the upwelling of the upper mantle pushing the lower crust of the fluvial graben upwards; the yellow area is the area where the density decreases after heating at the bottom of the lithosphere in the northern Ordos block; the orange area shows the ductile flow of the lower crust, which thickens the lower crust of the Ordos block; orange also indicates a high Vp/vs. ratio; the red arrows in the thickened lower crust indicate the direction of ductile flow; and grey indicates thick sedimentary basins beneath the Hetao Basin (Tian et al., 1992).

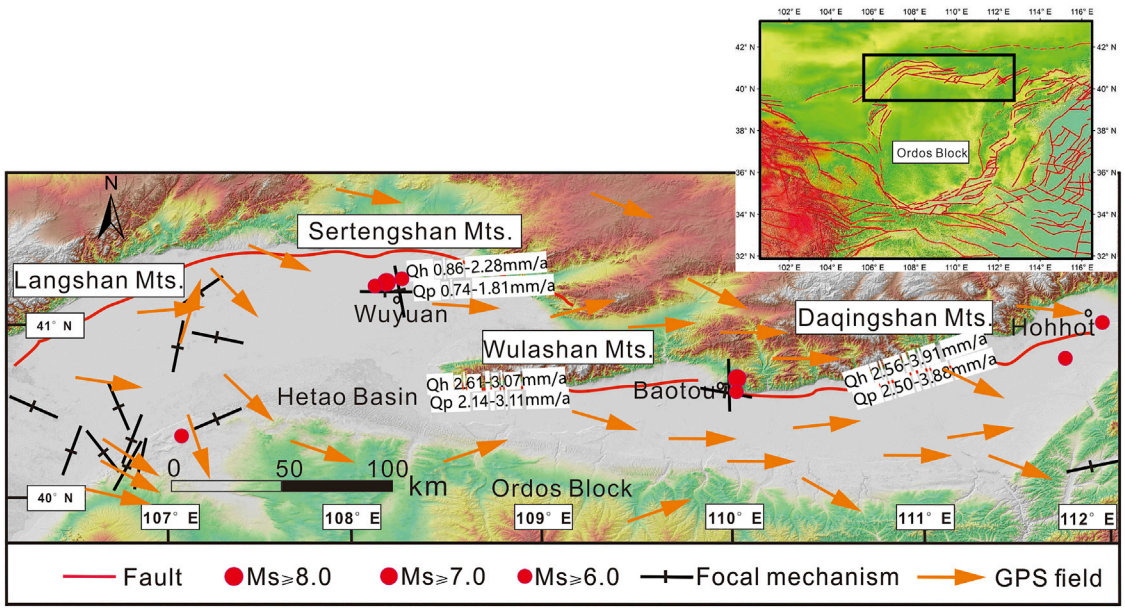

FIGURE 8 | Modern regional tectonic stress field in the Hetao Basin.

belt began to form. Here, upwelling of deep material beneath the basin played an important role (**Figure 7D**). Therefore, the combined action of the regional horizontal stress field and vertical force generated by deep material movement characterized the dynamic conditions associated with neotectonic activity in this area (Deng and You, 1985).

During the Cenozoic period, the Hetao Basin experienced heavy sedimentation, with the thickness of deposited sediments reaching thousands of metres. Li and Nie (1987) estimated the thickness of the Cenozoic floor based on petroleum geology, hydrology and seismic data and field data (**Figure 7A**). In the Quaternary period, the boundary faults of the Hetao Basin were highly active, and the faulted basin was constantly subsiding. The depositional centre was always located near the piedmont fault in the north. According to petroleum geology and seismic data, the thickness of the Quaternary strata in the Hetao Basin is large in the west and small in the east (Research Group of Active Fault System around Ordos Massif, 1988) (**Figure 7B**). **Figures 7A,B** show that the sedimentary thickness of the Linhe Basin has been much greater than that of the Huhe Basin since the Cenozoic, indicating that the Linhe Basin was the depositional centre of the Hetao Basin in the Cenozoic. However, during the Quaternary, the fault activity on the northern margin of the Hetao Basin has been strong. During this time, the sedimentary thickness of the Linhe Basin has been similar to that of the Huhe Basin, which indicates that the faults on the northern margin controlled the deposition in the Hetao Basin to a certain extent. Based on the increasing fault slip rate from west to east along the northern margin of the Hetao Basin, we infer that the depositional centre of the Hetao Basin has migrated from west to east during the Quaternary. In addition, the depth of the Moho surface in the Hetao Basin varies greatly, with obvious block characteristics. Overall, the crustal thickness gradually increases from east to west, consistent with its geological structural characteristics (Feng et al., 2015) (**Figure 7C**). The Yinshan range is mainly characterized by an upper mantle zone, and two mantle zone centres have formed in the Langshan and Daqingshan areas. The crustal thickness of the Langshan area is greater than that of the Daqingshan area, and in the Yinshan range, the crustal thickness is thicker in the west and thinner in the east, as is the overall isobath (Yang et al., 2016). Feng et al. (2015) studied the deep seismic reflection profile of this basin and found that a lithospheric deep fault was located beneath the Daqingshan piedmont fault, which extended from the upper crust, cut the middle-lower crust and Moho surface and entered the upper mantle. The existence of deep faults provides channels for upwelling and intense energy exchange with deep hot material (**Figure 7C**). The movement of upwelling magmatic material in the asthenosphere caused the melting or softening of the lithosphere in the lower crust and upper mantle of the Hetao fault zone (Yao, 2014). Therefore, we conclude that the depositional centre of the Hetao Basin has tended to migrate from west to east. The vertical force generated by deep material movement may have led to a greater vertical slip rate along the fault zone in the eastern portion of the northern margin of the Hetao Basin (**Figure 7C**).

Previous studies on the tectonic stress field of the fault zone around the Ordos block suggest that the tectonic stress on the

northern margin of the Ordos block is NW-SE tensile stress (Deng et al., 1999; Fan et al., 2003; Xie et al., 2004; Zhao et al., 2016; Qu et al., 2017). Based on the Crustal Stress Database (2015) of the National Institute of Natural Hazards, Ministry of Emergency Management, we prepared a map of the average modern stress field in the Hetao Basin area. The modern tectonic stress field shows that the Hetao Basin is controlled by NE-SW compression and NW-SW extension. The main compressive stress axis and the tensile stress axis are approximately horizontal, and the direction of the tensile stress axis is 138.66° (**Figure 8**).

Although the active faults on the northern margin of the Hetao Basin are in the same tectonic stress field, the stress trends of the active faults are different. Therefore, the influence of tensile stress on active faults is different. In addition, the angle between the tensile stress axis and fault strike affects the slip component and dip slip rate of the tensile stress. When the angle between the tensile stress axis and the fault strike is 90°, the slip component and dip slip rate of the tensile stress are the maximum. When the angle between the tensile stress axis and the fault strike increases, the dip slip rate of the tensile stress increases, and the strike-slip rate of the extensional stress decreases. As shown in **Supplementary Table S6**, by comparing the angle between the extensional stress axis and the fault strike in the four faults and the corresponding maximum vertical slip rate, we find that the vertical slip rates of the Sertengshan piedmont fault, Wulashan piedmont fault and Daqingshan piedmont fault gradually increase from west to east under the influence of the modern stress field, which strictly agrees with the theory. However, the angle between the extensional stress axis and the fault strike for the Daqingshan piedmont fault is smaller than that for the Langshan piedmont fault, and the maximum vertical slip rate is larger than that of the Langshan piedmont fault. We believe that this is consistent with our prediction that the vertical force generated by deep material movement may lead to a greater vertical slip rate along the fault zone in the eastern portion of the northern margin of the Hetao Basin. That is, the vertical force generated by deep material movement is the dominant factor that leads to the larger vertical slip rate in the eastern portion of the Hetao Basin. Under the combined action of the modern stress field in the Hetao Basin and vertical force generated by deep material movement, the vertical slip rates of the Sertengshan piedmont fault, Wulashan piedmont fault and Daqingshan piedmont fault increase from west to east, exhibiting spatial variation.

6 CONCLUSION

In this paper, the vertical slip rates were calculated using the vertical displacements of fault-adjacent footwall terraces and the corresponding strata in hanging wall boreholes. The vertical displacement calculated by using the marker strata of both fault walls is not affected by the surface sediment cover, and the calculated vertical slip rate is complete and accurate. However, our vertical slip rate includes the interseismic creep slip rates of the fault. The vertical slip rates of the three active faults on the northern margin of the Hetao Basin since the late Pleistocene and Holocene increase from west to east. The fault activity of the Sertengshan piedmont fault increased from the late Pleistocene to the Holocene, but that of the Daqingshan piedmont fault and Wulashan piedmont fault decreased during this period. Based on the recurrence characteristics of palaeoearthquakes and the vertical slip rates obtained in this paper, it can be found that the Langshankou and Hongqicun segments of the Sertengshan piedmont fault are at higher risk of earthquakes than other segments. Among the fault segments of the Wulashan piedmont fault, the possibility of future earthquakes in the Baotou segment is high. The seismic risk of the Tuyouxi segment of the Daqingshan piedmont fault should not be ignored, and the Tuzuoxi, Bikeqi and Hohhot segments have high seismic risk. Based on the dynamic model of the formation and evolution of the Ordos block and its adjacent fault basins, it is concluded that the depositional centre of the Hetao basin has tended to migrate from west to east during the Quaternary. The vertical force generated by deep material movement is the dominant factor leading to a greater vertical slip rate along the fault zone in the eastern portion of the northern margin of the Hetao Basin. The modern stress field in the Hetao Basin results in an increasing vertical slip rate of active faults from west to east on the northern margin of the basin.

DATA AVAILABILITY STATEMENT

The raw data supporting the conclusion of this article will be made available by the authors, without undue reservation.

AUTHOR CONTRIBUTIONS

ZH designed the project. ZH, DX, JL, HZ and KL performed the fieldwork. DX and ZH analysed all the data and wrote the first draft. All authors discussed the results, provided feedback and commented on the manuscript.

FUNDING

This work was supported by a research grant from the National Institute of Natural Hazards, Ministry of Emergency Management of China (ZDJ 2019-21), and grants from the National Science Foundation of China (Nos. 41872227 and 41602221).

ACKNOWLEDGMENTS

We thank the reviewers and editors for their help with improving the manuscript. The optically stimulated luminescence (OSL) samples were analysed by Zhao-Junxiang at the Key Laboratory of Crustal Dynamics (National Institute of Natural Hazards, Ministry of Emergency Management of China). ^{14}C sample testing was conducted by the BETA Laboratory in the United States.

SUPPLEMENTARY MATERIAL

The Supplementary Material for this article can be found online at: https://www.frontiersin.org/articles/10.3389/feart.2022.816922/full#supplementary-material

REFERENCES

Aitken, M. J. (1998). *An Introduction to Optical Dating*. Oxford: Oxford University Press.

Bevis, M., and Isacks, B. L. (1981). Leveling Arrays as Multicomponent Tiltmeters: Slow Deformation in the New Hebrides Island Arc. *J. Geophys. Res.* 86, 7808–7824. doi:10.1029/jb086ib09p07808

Chen, F. H., Fan, Y. X., and Chun, X. (2008). Preliminary Study of the "Jilantai-Hetao" Megalake in Late Quaternary. *Sci. Bull.* 53, 1207–1219. doi:10.1007/s11434-008-0227-3

Chen, L. C. (2002). *Paleoearthquakes, the Law of Strong Earthquake Recurrence and Potential Sites for the Occurrence of Future Strong Earthquakes in the Hetao Fault-Depression Zone*. Beijing, China: Institute of Geology, China Earthquake Adaministration. Master Thesis.

Chen, L., Cheng, C., and Wei, Z. (2009). Seismic Evidence for Significant Lateral Variations in Lithospheric Thickness beneath the central and Western North China Craton. *Earth Planet. Sci. Lett.* 286, 171–183. doi:10.1016/j.epsl.2009.06.022

Deng, Q. D., Cheng, S. P., and Min, W. (1999). Discussion on Cenozoic Tectonics and Dynamics of Ordos Block. *J. Geomech* 5, 20–26.

Deng, Q. D., and You, H. C. (1985). *The Structure Activity and Formation Mechanism of the Down-Faulted Basins Around the Ordos Block. Research on Recent Crustal Movement, 1*. Beijing, China: Continental Rift and Deep Internal Processes Beijing: Seismological Press, 58–78.

Dong, S. P. (2015). *Late Quaternary Tectonic Activity and Paleoseismology along the Langshan Range-Front Fault*. Beijing, China: Institute of Geology, China Earthquake Administration.

Du, F., Wen, X. Z., and Zhang, P. Z. (2010). Post-seismic Slip and Deformation on the Luhuo Segment of the Xianshuihe Fault Zone. *Chin. J. Geophys.* 53, 2355–2366.

Fan, J. X., Ma, J., and Diao, G. (2003). Tectonic Stress Field Around Ordos Obtained from the Focal Mechanism Solution of Small Earthquakes. *Seismol. Geol.*, 88–99.

Feng, S. Y., Liu, B. J., Ji, J. F., He, Y. J., Tan, Y. L., and Li, Y. Q. (2015). The Survey on fine Lithospheric Structure beneath Hohhot-Baotou basin by Deep Seismic Reflection Profile. Chin. *J. Geophys. (Acta Geophys. Sin.)* 58, 1158–1168. doi:10.6038/cjg20150406

Gao, S., Rudnick, R. L., Yuan, H.-L., Liu, X.-M., Liu, Y.-S., Xu, W.-L., et al. (2004). Recycling Lower continental Crust in the North China Craton. *Nature* 432, 892–897. doi:10.1038/nature03162

He, X. L., Zhang, X. J., He, Z. X., and Jia, L. Y. (2015). Development Features of the Late Quaternary Debris Flow and Their Tectonic Significance in Langshan Area Inner Mongolia. *Geol. Bull. China* 34 (9), 1735–1748.

He, Z., Ma, B., Hao, Y., Zhao, J., and Wang, J. (2020). Surface Rupture Geomorphology and Vertical Slip Rates Constrained by Terraces along the Wulashan piedmont Fault in the Hetao basin, China. *Geomorphology* 358, 107116. doi:10.1016/j.geomorph.2020.107116

He, Z., and Ma, B. (2015). Holocene Paleoearthquakes of the Daqingshan Fault Detected from Knickpoint Identification and Alluvial Soil Profile. *J. Asian Earth Sci.* 98, 261–271. doi:10.1016/j.jseaes.2014.11.025

He, Z., Ma, B., Long, J., Wang, J., and Zhang, H. (2018). New Progress in Paleoearthquake Studies of the East Sertengshan Piedmont Fault, Inner Mongolia, China. *J. Earth Sci.* 29, 441–451. doi:10.1007/s12583-017-0937-z

He, Z. T. (2006). Occurrence Probability of Characteristic Earthquakes on the Segments of Daqingshan piedmont Fault. J. *Anthol. Crustal Struct. Crustal Stress*, 35–41.

He, Z. T., Ma, B. Q., and Lu, H. F. (2007). Segmentation of Active Fault Zones and Potential Focal Areas in the Piedmont of Daqing Mountain. Seismol. *Geol*, 765–775.

He, Z. X., Zhang, X. J., He, Z. X., and Jia, L. Y. (2014). Genesis of Piedmont Terraces and its Neotectonics Movement Significance in Langshan Mountain Area, Inner Mongolia. *Geoscience* 28 (1), 98–108.

Huang, Z., Li, H., Zheng, Y., and Peng, Y. (2009). The Lithosphere of North China Craton from Surface Wave Tomography. *Earth Planet. Sci. Lett.* 288, 164–173. doi:10.1016/j.epsl.2009.09.019

Institute of Crustal and Dynamics, China Earthquake Administration, (1994). 1: 50000 Geological Mapping and Comprehensive Research of Daqingshan Piedmont Fault.

Institute of Crustal and Dynamics, China Earthquake Administration, (1995). 1: 50000 Geological Mapping and Comprehensive Research of Langshan-Sertengshan Piedmont Fault.

Institute of Crustal and Dynamics, China Earthquake Administration, (2013). 1: 50000 Geological Mapping and Comprehensive Research of Wulashan Piedmont Fault.

Lee, J.-C., Angelier, J., Chu, H.-T., Hu, J.-C., and Jeng, F.-S. (2001). Continuous Monitoring of an Active Fault in a Plate Suture Zone: A Creepmeter Study of the Chihshang Fault, Eastern Taiwan. *Tectonophysics* 333, 219–240. doi:10.1016/s0040-1951(00)00276-6

Li, K., and Nie, Z. S. (1987). Formation and Evolution of Fault Depression in Hetao Area and Seismic Activity. *Crustal Tecton. Crustal Stress*, 42–53.

Liang, J. P., Xie, F. R., and Li, K. (1997). "The Character of Tectonic Stress Field, Structural Movement and Seismicity in Daqing Mountain Area," in *Institute of Crustal Dynamics, China Earthquake Administration*. Editors Crustal. Tectonics and Crustal. Stress (Beijing, China: Seismological Press), 87–96.

Liang, K. (2019). Late Quaternary Tectonic Activity Characteristics of the Northwestern Margin of the Ordos Block. Institute of Geology, China Earthquake Administration.

Lienkaemper, J. J., Barry, G. R., Smith, F. E., Mello, J. D., and McFarland, F. S. (2013). The Greenville Fault: Preliminary Estimates of its Long-Term Creep Rate and Seismic Potential. *Bull. Seismological Soc. America* 103, 2729–2738. doi:10.1785/0120120169

Lienkaemper, J. J., Galehouse, J. S., and Simpson, R. W. (2001). Long-term Monitoring of Creep Rate along the Hayward Fault and Evidence for a Lasting Creep Response to 1989 Loma Prieta Earthquake. *Geophys. Res. Lett.* 28, 2265–2268. doi:10.1029/2000gl012776

Lienkaemper, J. J., Mcfarland, F. S., Simpson, R. W., and Caskey, S. J. (2014). Using Surface Creep Rate to Infer Fraction Locked for Sections of the San Andreas Fault System in Northern California from Alignment Array and GPS Data. *Bull. Seismological Soc. America* 104, 3094–3114. doi:10.1785/0120140117

Lisowski, M., and Prescott, W. H. (1981). Short-range Distance Measurements along the San Andreas Fault System in central California, 1975 to 1979. *Bull. Seismological Soc. America* 71, 1607–1624. doi:10.1785/bssa0710051607

Liu, M., Cui, X., and Liu, F. (2004). Cenozoic Rifting and Volcanism in Eastern China: a Mantle Dynamic Link to the Indo-Asian Collision? *Tectonophysics* 393, 29–42. doi:10.1016/j.tecto.2004.07.029

Liu, Q. (2012). Structural Deformation Characteristics of Daqingshan piedmont Fault in Inner Mongolia. *J. World Geol.* 31, 113–119.

Liu, Z., Zhao, H., Wang, C. M., Ji, Y., Zhang, Y., Liu, L., et al. (2014). OSL Ages of Sedimentary Layers in Linhe Depression since Late Pleistocene. *Arid Land Geogr.* 37, 439–446.

Long, J. Y., He, Z. T., Zhang, H., and Ma, B. Q. (2017). Characteristics of Structural Geomorphology and Segmentation of Sertengshan piedmont Fault from Dahoudian to Wayaotan. *Geoscience* 31, 71.

Ma, B. Q., Sheng, X. Q., and Zhang, S. R. (1998). "Late Quaternary Activities of the Wulashan piedmont Fault," in *Institute of Crustal Dynamics, China Earthquake Administration*. Editors Crustal. Tectonics and Crustal. Stress (Beijing, China: Seismological Press), 22–27.

Murray, A. S., and Wintle, A. G. (2003). The Single Aliquot Regenerative Dose Protocol: Potential for Improvements in Reliability. *Radiat. Measurements* 37, 377–381. doi:10.1016/s1350-4487(03)00053-2

Northrup, C. J., Royden, L. H., and Burchfiel, B. C. (1995). Motion of the Pacific Plate Relative to Eurasia and its Potential Relation to Cenozoic Extension along the Eastern Margin of Eurasia. *Geology* 23, 719–722. doi:10.1130/0091-7613(1995)023<0719:motppr>2.3.co;2

Qian, R. (2014). The Understanding of Using and Development in Radiocarbon Dating. J. *Qiqihar Jr. Teach. Coll.*, 112–113.

Qu, W., Lu, Z., Zhang, M., Zhang, Q., Wang, Q., Zhu, W., et al. (2017). Crustal Strain fields in the Surrounding Areas of the Ordos Block, central China, Estimated by the Least-Squares Collocation Technique. *J. Geodynamics* 106, 1–11. doi:10.1016/j.jog.2017.01.005

Ran, Y. K., Zhang, P. Z., and Chen, L. C. (2003). Research on the Completeness of Paleoseismic Activity History since Late Quaternary along the Daqingshan piedmont Fault in Hetao Depression Zone, North China. Earth Sci. *Front* 10, 207–216.

Research Group of Active Fault System around Ordos Massif (1988). *Active Fault System Around Ordos Massif*. Beijing, China: Seismological Press.

Sanchez, G. M., Rick, T. C., Culleton, B. J., Kennett, D. J., Buckley, M., Erlandson, J. M., et al. (2018). Radiocarbon Dating Legacy Collections: A Bayesian Analysis of High-Precision AMS 14C Dates from the Par-Tee Site, Oregon. *J. Archaeological Sci. Rep.* 21, 833–848. doi:10.1016/j.jasrep.2018.08.033

Savage, J. C., Prescott, W. H., Lisowski, M., and King, N. (1979). Geodolite Measurements of Deformation Near Hollister, California, 1971-1978. *J. Geophys. Res.* 84, 7599–7615. doi:10.1029/jb084ib13p07599

Schulz, S. S., Mavko, G. M., Burford, R. O., and Stuart, W. D. (1982). Long-term Fault Creep Observations in central California. *J. Geophys. Res.* 87, 6977–6982. doi:10.1029/jb087ib08p06977

Shi, W., Dong, S., and Hu, J. (2020). Neotectonics Around the Ordos Block, North China: a Review and New Insights. *Earth-Science Rev.* 200, 102969. doi:10.1016/j.earscirev.2019.102969

Sun, A. Q., Hu, X., and Niu, S. Y. (1990). Geological Features of Active Structure in Langshan Area, Nei Mongol. *J. Hebei Coll. Geology.* 13 (1), 27–35.

Sun, C. B. (2012). Combination of Trenching and Drilling to Detect Paleo-Seismic Events on Concealed Active Faults: Taking Tangshan Fault as an Example. *Crustal Tecton. Crustal Stress*, 147–155.

Tao, S. X. (2020). *Holocene Lake Environmental Changes in the East Asian Summer Monsoon Limit Revealed by Lake Geomorphy and Lacustrine Sediment Core Record from the Wulanhushao Lake Basin.* Lanzhou, China: Lanzhou University.

Teng, J. W., Wang, F. Y., Zhao, W. Z., Zhang, Y. Q., Zhang, X. K., Yan, Y. F., et al. (2010). Velocity Structure of Layered Block and Deep Dynamic Process in the Lithosphere beneath the Yinshan Orogenic belt and Ordos Basin. *Chin. J. Geophys.* 53, 67–85. doi:10.3969/j.issn.0001-5733.2010.01.008

Tian, Z.-Y., Han, P., and Xu, K.-D. (1992). The Mesozoic-Cenozoic East China Rift System. *Tectonophysics* 208, 341–363. doi:10.1016/0040-1951(92)90354-9

Wang, J., and He, Z. (2020). Responses of Stream Geomorphic Indices to Piedmont Fault Activity in the Daqingshan Area of China. *J. Earth Sci.* 31 (5), 978–987. doi:10.1007/s12583-020-1321-y

Wang, L., Zhang, Q., Li, X., Zhang, Y., Guan, J. A., and Tu, R. (2011). Dynamic and Real Time Deformation Monitoring of Landslide with GPS-RTK Technology. *J. Eng. Geol.* 19, 193–198.

Wu, W. M., Li, K., Ma, B. Q., Sheng, X. Q., and Yang, F. (1996). Study on Quaternary Activity of Daqingshan Piedmont Fault Zone. *Crustal Tecton. Crustal Stress*, 1–10.

Xie, F.-R., Cui, X.-F., Zhao, J.-T., Chen, Q.-C., and Li, H. (2004). Regionalization of the Recent Tectonic Stress Field in China and Adjacent Regions. *Chin. J. Geophys.* 47, 745–754. doi:10.1002/cjg2.3545

Xu, X. W., Bai, L. X., Wei, L. M., Chen, G., and Yu, G. (2019). Discussion on Initiation Time of the Latest Tectonic Movement in Break-Up Region of the North China Craton. *Earth Sci.* 44, 1647–1660.

Yang, C. Y., Li, X. N., and Feng, X. J. (2021). The Late Quaternary and Present-Day Activities of the Kouzhen-Guanshan Fault on the Northern Boundary of Weihe Graben basin, china. *J. Seismology Geology.* 43, 504–520.

Yang, X. P., Ran, Y. K., Hu, B., and Guo, W. (2002). Active Fault and Paleoearthquakes of the piedmont Fault (Wujumengkou-Dongfeng Village) for Seertang Mountains, Inner Mongolia. *Earthq. Res. China* 18, 127–140.

Yang, Y. M., Zhang, G. Q., Chen, J., and Huang, R. B. (2016). Moho Depth Distribution Character beneath the Ordos Block's Northern Margin Areas and Surrounding Regions. *J. Seismol. Geomagn. Obs. Res.* 37, 1–8. doi:10.3969/j.issn.1003-3246.2016.06.001

Yao, Z. X. (2014). *Rayleigh Wave Phase Velocities and Azimuthal Anisotropy beneath Ordos Block and its Surrounding Areas. Institute of Geophysics*. Beijing, China: China Earthquake Administration.

Zhang, H. (2017). *Study on the Activity of Sertengshan Piedmont Fault Zone in Late Quaternary*. Beijing, China: Institute of Crustal and Dynamics, and China Earthquake Administration.

Zhang, H., He, Z., Ma, B., Long, J., Liang, K., and Wang, J. (2017). The Vertical Slip Rate of the Sertengshan piedmont Fault, Inner Mongolia, China. *J. Asian Earth Sci.* 143, 95–108. doi:10.1016/j.jseaes.2017.04.014

Zhang, J., Wen, X.-z., Cao, J.-l., Yan, W., Yang, Y.-l., and Su, Q. (2018). Surface Creep and Slip-Behavior Segmentation along the Northwestern Xianshuihe Fault Zone of Southwestern China Determined from Decades of Fault-Crossing Short-Baseline and Short-Level Surveys. *Tectonophysics* 722, 356–372. doi:10.1016/j.tecto.2017.11.002

Zhang, P. Z., Deng, Q. D., Zhang, Z. Q., and Haibing, Li. (2013). Active Faults, Earthquake Hazards and Associated Geodynamic Processes in continental China. *Sci. Sin. Terrae* 43, 1607–1620. doi:10.1360/zd-2013-43-10-1607

Zhang, Y. Q., Liao, C. Z., Shi, W., and Hu, B. (2006). Neotectonic Evolution of the Peripheral Zones of the Ordos basin and Geodynamic Setting. *Geol. J. China Univ.* 12, 285–297.

Zhang, Y. Q., Shi, W., and Dong, S. W. (2019). Neotectonics of North China: Interplay between Far-Field Effect of India-Eurasia Collision and Pacific Subduction Related Deep-Seated Mantle Upwelling. *J. Acta Geol. Sin* 93, 971–1001. doi:10.1111/1755-6724.14187

Zhao, M., Shen, G.-J., He, J.-N., Cao, B., and Li, H.-C. (2017). AMS 14C Dating of the Hominin Archaeological Site Chuandong Cave in Guizhou Province, Southwestern China. *Quat. Int.* 447, 102–110. doi:10.1016/j.quaint.2017.04.037

Zhao, W., Hou, G., and Hari, K. R. (2016). Two Episodes of Structural Fractures and Their Stress Field Modeling in the Ordos Block, Northern China. *J. Geodynamics* 97, 7–21. doi:10.1016/j.jog.2016.02.005

Zhu, R., Xu, Y., Zhu, G., Zhang, H., Xia, Q., and Zheng, T. (2012). Destruction of the North China Craton. *Sci. China Earth Sci.* 55, 1565–1587. doi:10.1007/s11430-012-4516-y

Conflict of Interest: The authors declare that the research was conducted in the absence of any commercial or financial relationships that could be construed as a potential conflict of interest.

Publisher's Note: All claims expressed in this article are solely those of the authors and do not necessarily represent those of their affiliated organizations, or those of the publisher, the editors, and the reviewers. Any product that may be evaluated in this article, or claim that may be made by its manufacturer, is not guaranteed or endorsed by the publisher.